# Epigenetic insights into GABAergic development in Dravet Syndrome iPSC and therapeutic implications

Jens Schuster [1,#], Xi Lu[1, #], Yonglong Dang[1,#], Joakim Klar[1], Amelie Wenz[1], Niklas Dahl[1,*], Xingqi Chen[1,*]

[1]Department of Immunology, Genetics and Pathology, Uppsala University and Science for Life Laboratory, Uppsala, Sweden

# Equal contribution

* Corresponding author: xingqi.chen@igp.uu.se or niklas.dahl@igp.uu.se

**Key words**

Dravet syndrome, epilepsy, Chromatin accessibility, iPSC modeling, neuronal differentiation, epigenetic profiling, valproic acid

**Abstract**

Dravet syndrome (DS) is a devastating early onset refractory epilepsy syndrome caused by variants in the *SCN1A* gene. A disturbed GABAergic interneuron function is implicated in the progression to DS but the underlying developmental and pathophysiological mechanisms remain elusive, in particularly at the chromatin level. In this study, we utilized induced pluripotent stem cells (iPSCs) derived from DS cases and healthy donors to model disease-associated epigenetic abnormalities of GABAergic development. Employing the ATAC-Seq technique, we assessed chromatin accessibility at multiple time points (Day 0, Day 19, Day 35, and Day 65) of GABAergic differentiation. Additionally, we elucidated the effects of the commonly used anti-seizure drug valproic acid (VPA) on chromatin accessibility in GABAergic cells. The distinct dynamics in chromatin profile of DS iPSC predicted accelerated early GABAergic development, evident at D19, and diverged further from the pattern in control iPSC with continued differentiation, indicating a disrupted GABAergic maturation. Exposure to VPA at D65 reshaped the chromatin landscape at a variable extent in different iPSC-lines and rescued the observed dysfunctional development in some DS iPSC-GABA. This study provides the first comprehensive investigation on the chromatin landscape of GABAergic differentiation in DS-patient iPSC, offering valuable insights into the

epigenetic dysregulations associated with interneuronal dysfunction in DS. Moreover, our detailed analysis of the chromatin changes induced by VPA in iPSC-GABA holds the potential to improve development of personalized and targeted anti-epileptic therapies.

## Introduction/Background

Dravet syndrome (DS) is an early onset and intractable epilepsy with an unfavorable long-term outcome. The first seizures are usually triggered by fever within the first 12 months of life[1,2]. Characteristic clinical features are age-related progression of seizures, cognitive decline, behavioral problems and movement disorder. The complex neurological symptoms associated with DS suggest underlying pathophysiological mechanisms that interfere with brain development[1-4]. Approximately 80% of DS cases carry heterozygous variants in the *SCN1A* gene encoding the α-subunit voltage-gated sodium channel (Nav1.1)[1,5]. Prior insights on the neuropathophysiology in DS have come from the *Scn1a* heterozygous mice, indicating a vital role of cortical interneurons in the pathogenesis. Mice with Nav1.1 haploinsufficiency in GABAergic interneurons exhibit spontaneous seizures and behavioral abnormalities[6-9] that are associated with subnormal sodium currents and impaired excitability of inhibitory interneurons[10,11]. Additionally, human iPSC derived neural cells carrying distinct *SCN1A* mutations have recapitulated electrophysiological and molecular perturbations in DS[12-16]. In combination, these studies have confirmed that *SCN1A* variants cause delayed sodium currents in activated and mainly inhibitory GABAergic interneurons, supporting the notion that seizures in DS are caused by deficient cortical inhibition[12].

Interneuronal progenitors emerge from the embryonic subpallium, mainly the median ganglionic eminence, and migrate tangentially to cortical progenitor zones. The second half of gestation is a period of rapid development of the human cortical GABAergic system that continues after term[17,18]. The extended developmental processes into mature GABAergic interneurons require continuous and complex remodeling of the chromatin structure for transcriptional adaptations[19]. While it is now clear that the distinct features in DS is associated with a reduced sodium current density in Nav1.1 haploinsufficient interneurons and a disinhibition of the cortical network[6,13,20], the underlying epigenetic mechanisms are poorly understood.

68 Treatment of DS patients is challenging and seizure control is rarely attainable[21]. The most
69 frequently used first-line drug is valproic acid (VPA)[1]. However, more than 50% of DS
70 patients are drug resistant without any decrease in seizure-frequency upon treatment[1],
71 indicating endogenous and subject-specific responses to VPA. The mechanisms by which
72 VPA act are not fully understood, but studies suggest that the drug inhibits histone
73 deacetylase (HDAC) with an impact on chromatin structure and gene expression[22,23].
74 Furthermore, a direct interaction of VPA with sodium- or calcium-gated ion channels (e.g.
75 Nav1.1) and enzymes crucial for GABA turnover has been proposed[22]. While these studies
76 have brought important information on the mode of action of VPA[24-28], the specific effects of
77 VPA on chromatin architecture of inhibitory GABAergic interneurons have not yet been
78 investigated to our knowledge.
79
80 We recently established induced pluripotent stem cell (iPSC) lines carrying distinct disease-
81 causing mutations in the *SNC1A* and modeled GABAergic interneuron development in DS[13,29].
82 The DS-patient derived iPSC recapitulated electrophysiological abnormalities and gene
83 expression analysis showed enrichment for histone modifications, suggesting epigenetic
84 abnormalities[13]. We therefore sought to explore the dynamics of open chromatin in our DS-
85 model of GABAergic development in DS using the assay of transposase accessible chromatin
86 sequencing (ATAC-Seq). The methodology has previously been used to study chromatin
87 accessibility of annotated genes during brain development[30-32] and, specifically, in
88 interneuronal differentiation[19,33]. Herein, we employed ATAC-Seq to investigate the
89 dynamics of chromatin accessibility in iPSC of DS-patients and healthy donors at four
90 different time points (Day 0, Day 19, Day 35, and Day 65) of GABAergic development.
91 Moreover, we explored the effect of VPA on chromatin accessibility in GABAergic neurons.
92 Our study uncovered accelerated chromatin changes in DS patient iPSC during the initial
93 phase of GABAergic development (up to Day 19) when compared to iPSC of healthy donors.
94 Further differentiation revealed that DS-patient GABAergic cells acquire a distinct chromatin
95 profile when compared to that of control cells. Notably, VPA treatment of GABAergic
96 neurons leads to unspecific genome-wide changes in chromatin architecture that predicts a
97 promoted GABAergic development in some iPSC lines. This study represents the first
98 investigation of the chromatin dynamics of GABAergic development in DS-patient iPSC,
99 shedding light on the underlying epigenetic abnormalities. Moreover, the in-depth
100 characterization of chromatin changes in GABAergic neurons induced by VPA may bring
101 important information for the development of individualized anti-seizure therapies.

102

103 **Results**

104 **Dynamic chromatin accessibility in an iPSC model of GABAergic development**

105 We first obtained a reference for chromatin accessibility changes during GABAergic
106 interneuronal differentiation in iPSC from three healthy donors (Ctl) using ATAC-Seq[34]
107 (**Figure 1A**). The differentiating cultures were collected at four distinct time points of
108 differentiation at day 0 (D0; termed iPSC), D19 (neural progenitor cells; NPC), D35
109 (intermediate neuronal cells; imN) and D65 (GABAergic interneurons; GABA). The cultures
110 displayed expression of marker genes confirming the development into GABAergic
111 interneurons. At D0, cultures stained positive for pluripotent stem cell markers such as
112 NANOG, SOX2, and OCT4. The expression of these markers decreased upon neural
113 induction and disappeared with further differentiation. Markers for neural progenitor cells
114 (FOXG1, PAX6) were expressed at D19 followed by the expression of immature neuronal
115 cell markers (DCX and NKX2.1) at D35 and of markers for GABAergic interneurons (GAD1,
116 TUBB3) at D65 (**Supplementary Figure 1A**).

117

118 The quality of ATAC-Seq data from each sample was validated (**Supplementary Figure 1B**)
119 by the transcription start site enrichment score (**Supplementary Figure 1C**) and by
120 calculating the fraction of reads in enriched peaks (FRiP) (**Supplementary Figure 1D**). We
121 captured accessible chromatin peaks at each time-point of differentiation: 58,382 peaks at D0
122 (Ctl-iPSC), 68,002 peaks at D19 (Ctl-NPC), 52,933 peaks at D35 (Ctl-iMN), and 74,561
123 peaks at D65 (Ctl-GABA). Genomic annotation of the accessible chromatin sites with respect
124 to promoters, introns and exons revealed a similar distribution in iPSC, NPC, imN and GABA
125 (**Supplementary Figure 1E).** Furthermore, principal component analysis (PCA) of chromatin
126 accessibility at the four time points demonstrated that the three biological replicates separated
127 into four clusters corresponding to each of the four time points of GABAergic development
128 (**Supplementary Figure 1F**), albeit with some degree of variability at the intermediate time
129 points (D19 (NPC) and D35 (imN)), possibly reflecting cell line specific and endogenous
130 differences reported previously[35]. We therefore treated the three Ctl-iPSC-lines as biological
131 replicates for downstream analysis.

132

133 We then characterized changes in chromatin accessibility during GABAergic development in
134 Ctl-iPSC. The ATAC-Seq peaks in iPSC (D0) were used as reference and compared to the
135 accessible peaks in NPC, imN and GABA. In total, we identified 19,931 significant

differential peaks (|log2(fold change (FC))|> 1, false discovery rate (FDR) < 0.01) (**Supplementary Figure 2A, Methods**). Next, we employed an unbiased cluster method to investigate the dynamics of these differential accessible peaks, resulting in the identification of four distinct clusters (Cluster 1-4) (**Figure 1B, Supplementary Figure 2A-C**). Cluster 1 (n=9,565) consisted of peaks that were open D0 (cluster Ctl-iPSC) and that gradually closed during differentiation. Cluster 2 (n=3,285) contained peaks that were predominantly open at D19 (cluster Ctl-NPC). Cluster 3 (n=3,533) exhibited a high chromatin accessibility at both D19 and D35 (cluster Ctl-imN) but more closed at D65. Cluster 4 (n=3,545) displayed the highest accessibility specifically at D65 (cluster Ctl-GABA; **Figure 1B, 1C**). A genomic annotation of the differential peaks in the four clusters with respect to promoters, exons, introns and distal regulatory sequences revealed differences mainly in introns and promoter regions. The Ctl-NPC cluster and Ctl-GABA cluster showed the highest proportion of open chromatin in introns (45.6% and 43.4%, respectively) whereas in the Ctl-iPSC and Ctl-imN clusters most accessible peaks were located in promoter regions (41.9% and 50.8%, respectively; **Figure 1D**).

We then performed transcription factor (TF) enrichment analysis on the differential peaks specific to each cluster (**Figure 1E**). The Ctl-iPSC cluster showed specific enrichment for motifs of TFs for pluripotency, such as BRN1, OCT6, among others (**Figure 1E**), whereas motifs for the SOX family of TFs were enriched in the Ctl-NPC-cluster. Ctl-NPC-specific transcription factor motifs (e.g., SOX family TFs) were detected in the NPC-specific cluster. Notably, motifs for common TFs (e.g., LHX family TFs, NKX6, RFX) as well as unique TFs (e.g. SOX9, NF1 and DLX3) were enriched in both the Ctl-imN-specific cluster and the Ctl-GABA specific cluster. The SOX family of TFs are important regulators of neuronal development[36] and DLX factors function in orchestrating transcriptional activity during cortical GABAergic development[37]. The temporal pattern of accessible and enriched TF motifs in our differentiating Ctl-iPSC cultures is thus consistent with the TFs required for neuronal and cortical GABAergic development *in vivo*, confirming our model system to be relevant.

Furthermore, we examined the biological processes associated with each cluster by assigning each differential peak to the nearest gene. The annotated genes were then used for KEGG analysis of each cluster (**Figure 1F**). In the Ctl-iPSC cluster we identified enrichment of pathways related to pluripotency, such as signaling regulating pluripotency of stem cells,

while the Ctl-GABA cluster showed exclusive enrichment for pathways for GABAergic neurons, such as GABAergic synapse and Neurotrophin signaling (**Figure 1F**). Genome traces of annotated genes in each cluster validated the differential accessible chromatin, e.g. for *NANOG* in the Ctl-iPSC cluster, *PAX6* and *GAD2* in the Ctl-NPC and Ctl-imN clusters, respectively, and *GABRG3* in the Ctl-GABA cluster (**Figure 1G**). Taken together, these findings show that the captured chromatin dynamics comply with the induction and development of GABAergic neurons.

**Dynamic chromatin accessibility in a DS-iPSC model of GABAergic development**

Next, to gain a deeper understanding of chromatin dynamics during GABAergic development associated with DS, we used the same strategy as above for differentiation and ATAC-Seq analysis of iPSC-lines derived from the three DS patients (**Figure 2A, Supplementary Figure 3A**). Unfortunately, one of the DS-iPSC lines (DD4A) did not differentiate up to D65 for unknown reasons why data at this specific time-point are based on two DS-iPSC lines.

The ATAC-Seq data showed high quality and reproducibility at all four time-points (**Supplementary Figure 3B-D**). In total, we detected 89,363 peaks in DS-iPSC, 79,270 peaks in DS-NPC, 113,519 peaks in DS-imN, and 41,665 peaks in DS-GABA. The genomic distribution of these accessible chromatin peaks with respect to promoters, introns and exons showed deviations when compared to Ctl-iPSC lines, mainly at D35 (DS-imN) and at D65 (DS-GABA) (**Supplementary Figure 3E**). However, the proportion of peaks at promoter regions increased from 28.5% in DS-imN to 44.6% in DS-GABA, while the peaks at introns decreased from 40.0% to 31.3%, respectively. Furthermore, the PCA of chromatin accessibility in DS-iPSC replicates showed that they clustered together at D0, D19 and D35 (**Supplementary Figure 3F**). Notably, the clusters at D19 (iPSC-NPC) and at D35 (iPSC-imN) showed a strong overlap in contrast to the well distributed clusters at all four time points in Ctl-iPSC lines (**Supplementary Figure 1F and 3F**). The different dynamics of chromatin accessibility of DS-iPSC lines when compared to that of Ctl-iPSC lines thus suggest a disrupted developmental trajectory into DS-GABAergic interneurons consistent with an altered function of inhibitory GABAergic interneurons in *Scn1a* heterozygous mice.

To further characterize chromatin changes in GABAergic differentiation of DS-iPSC lines, we used the same strategy as for Ctl-iPSC lines by using the profile of chromatin accessibility in DS-iPSCs (D0) as a reference. In total, we identified 19,896 differential peaks ($|\log2(FC)| > 1$, FDR $< 0.01$) (**Methods**) that were clustered into four groups using an unbiased approach.

204 The four DS-specific clusters showed similar patterns as those of the Ctl group. The number
205 of accessible peaks were 8,517 at D0 (DS-iPSC), 4,317 at D19 (DS-NPC), 3,579 at D35 (DS-
206 imN) and 3,483 at D65 (DS-GABA) (**Figure 2B, 2C, Supplementary Figure 4**). We
207 identified differences in the genomic distribution of the DS-iPSC clusters when compared to
208 that in the Ctl-iPSC clusters (**Figure 1D, 2D**). In the control group, 42.0% of the peaks were
209 located in promoter regions, whereas in the patient group, this proportion was slightly lower
210 at 37.3%. Additionally, a slightly higher proportion of DS-iPSC specific peaks were found in
211 intron regions (26.5%) compared to Ctl-iPSC (24.6%). The genomic features of the DS-NPC
212 specific cluster were similar between the Ctl group and the DS group. In the DS-imN specific
213 cluster, a lower proportion of peaks were located in promoter regions when compared to that
214 of the Ctl group (50.8% vs. 23.1%), while a lower proportion of peaks were from intron
215 regions in the Ctl group (27.8%) when compared to the DS group (46.2%). In the DS-GABA
216 and Ctl-GABA specific clusters, 34.7% and 25.9% of the peaks were located in promoter
217 regions, respectively, while 38.7% and 43.4% of the peaks were in intron regions in the Ctl
218 and DS groups, respectively.
219
220 We then examined the enrichment of motifs for trans-acting TFs within the differential peaks
221 of each DS-cluster at each time-point (**Figure 2E**). The DS-iPSC cluster specific peaks
222 showed enrichment of motifs from pluripotency related TFs, such as BRN1 and OCT4,
223 whereas TF motifs for the SOX family of TFs were enriched in both the DS-iPSC cluster and
224 DS-NPC cluster (**Figure 2E**). Peaks at TF motifs for LHX3 and NKX, specific for
225 GABAergic neurons were enriched only in the DS-NPC cluster but not in the DS-GABA
226 cluster. However, the DS-GABA specific peaks were enriched at motifs for the activator
227 protein-1 (AP-1) family of TFs, including JUN, FRA, and FOSL. Enriched motifs for the
228 BACH2 TF were observed only in the DS-GABA specific peaks and not in the Ctl-GABA
229 peaks. Together, these data further support that DS-iPSC, although they initially respond to
230 our protocol for GABAergic induction with accessible motifs for the SOX family of TFs,
231 have a disrupted trajectory into GABAergic interneurons as shown by the loss of motifs for
232 DLX and LHX at D65.
233
234 Next, we annotated the differential accessible peaks to nearby genes and performed KEGG
235 pathway analysis for each cluster (**Figure 2F**). Similar to Ctl-iPSC, the peaks of the DS-iPSC
236 specific cluster were enriched for pathways related to pluripotency. However, and in contrast
237 to the control group, pathways related to GABAergic synapse were enriched already in the

DS-NPC specific clusters but not in the later appearing clusters specific for DS-imN and DS-GABA (**Figure 2F**). Additionally, the pathway of long-term potentiation, a hallmark for mature GABAergic cells, was specifically enriched in the DS-imN specific cluster but not in the DS-GABA clusters. Furthermore, representative annotated genes for Ctl-iPSC lines, PAX6 and GAD2 in the Ctl-NPC and Ctl-imN clusters, and GABRG3 in the Ctl-GABA cluster, exhibit a different tendency of chromatin accessibility in DS-iPSC clusters (**Figure 2G**). The enrichment of TF motifs and predicted pathways relevant for GABAergic interneuron appearing already in DS-NPC, but not in DS-GABA, uncovered a pattern distinct from that in Ctl-iPSC lines, that strongly suggest a perturbed GABAergic development associated with *SCN1A* mutations.

**Common chromatin dynamics in Ctl- and DS-iPSC models of GABAergic development**

Identification of abnormal chromatin dynamics in GABAergic interneuronal development of DS-iPSC lines requires a thorough comparison with Ctl-iPSC lines. To extract shared dynamic chromatin features in DS-patient and Ctl-iPSC lines we first merged the differentially accessible chromatin peaks specific to each of the four time points (D0, D19, D35 and D65) within the Ctl and DS patient groups, respectively. The lists of all significant peaks in the Ctl- and DS- iPSC lines, respectively, were subsequently intersected to identify the common peak regions. In total, we identified 12,256 accessible chromatin peaks that show a shared and time-point specific pattern (**Figure 3A**).

Next, we sought to examine the genomic annotations, KEGG pathways, and TF motif enrichment for these common peaks (**Figure 3**). A K-mean clustering of read counts from the 12,252 accessible chromatin peaks revealed four common clusters (Com-1 with 6,264 peaks, Com-2 with 2,071 peaks, Com-3 with 1,793 peaks, and Com-4 with 2,124 peaks) (**Supplementary Figure 5**, **Figure 3A**). The DS-iPSC and Ctl-iPSC lines show a similar sequencing read count enrichment in Com-1 cluster and Com-2 clusters at the four time-points whereas slight differences are observed for the Com-3 and Com-4 clusters (**Figure 3A**). Accessible regions in Com-1 cluster are specifically open at D0 (iPSC) with annotations to TF genes for pluripotency such as *NANOG* and *SOX2*, among others. The Com-1 cluster remains closed at the following three time-points. The Com-2 cluster is closed at D0 but open at D19 (NPC) with accessible peaks at genes such as *MAP2*, *NEUROD1*, and *NEUROG1*, among others (**Figure 3A**).

In both the Ctl and DS-patient groups, accessible regions in the Com-3 cluster are closed D0 but slightly open at D19 (NPC) and at D35 (imN) and then more closed at D65 (GABA). However, the degree of openness for a large proportion of peaks is much higher in the DS-patient group when compared to the Ctl group. Furthermore, at D65 (GABA) the Com-3 cluster shows accessible regions at NPC-specific genes such as *MAP2* and *ATOH1* but not for regulatory elements of GABAergic neuron-specific genes, such as *ASCL1*, *LHX6*, and *DLX2*, among others. The absence of common open chromatin regions at regulatory elements for GABAergic specific genes in the Ctl and DS-patient groups supports altered dynamics of accessible chromatin at the late time-point GABAergic development in our model system.

The genomic distribution of accessible peaks with respect to promoters, exons and introns varies between the Com-clusters (**Figure 3B**). The Com-1 cluster shows a relatively large proportion of accessible chromatin regions from promoter regions (38.2%) when compared to the other clusters (Com-2: 22.0%; Com-3: 20.8%, and Com-4: 30.5%). Conversely, the Com-1 cluster shows a relatively small proportion of accessible regions in intronic regions (25.8%) when compared to Com-2, 3 and 4 clusters. However, the genomic distribution of accessible peaks was very similar in the Com-2 and Com-3 clusters.

We then conducted KEGG analysis on genes within peaks of the four Com-clusters to understand the common biological features of the Ctl- and DS-iPSC lines. We observed enrichment for the pathways of transcriptional regulation of pluripotency, that included *NANOG*, in Com-1 (**Figure 3C**) and of nitric oxide-stimulated guanylate cyclase that included *MAP2* in Com-2 (**Figure 3D**). However, in the Com-3 or Com-4 clusters, characterized by an increasing open chromatin with development, we did not find enrichment in pathways relevant for GABAergic cells (**Figure 3D**). These observations further indicate similarities in the Ctl and DS iPSC-lines in cellular processes up to D19 (NPC), but significant differences at D35 (imN) and D65 (GABA).

Furthermore, we examined the enrichment of motifs for trans-acting transcription factors (TFs) from all common peaks and clustered TFs with a k-means method. The TF enrichment patterns are similar in the Ctl and DS groups, and three TF clusters were observed. Cluster 1, containing pluripotent-specific TFs such as OCT4 and KLF, among others, shows enrichment at iPSC in both the control and DS patient groups (**Figure 3E, 3F**). Cluster 2, including TF motifs for the NPC-specific TFs ESRRB and HNF4A, is enriched in iPSC (D19) and imN

306 (D35) (**Figure 3E, 3F**), while some TFs relevant to GABAergic cells, such as NFAT and NF1,
307 are enriched in D65. No GABAergic neuron-specific TFs (e.g., DLX, LHX, ASCL) are
308 observed. Taken together, our data suggest similarities between Ctl- and DS-iPSC lines in
309 accessible chromatin at loci for TFs important for GABAergic induction and early
310 development. However, the Ctl- and DS-iPSC groups do not show similarities in the
311 enrichment of TFs that are critical at later stages of GABAergic maturation.
312
313 **Distinct chromatin features in DS-iPSC GABAergic development**
314 A PCA analysis of ATAC-Seq data at D0 demonstrated that profiles of chromatin
315 accessibility are similar in Ctl-iPSC and DS-iPSC-lines at d0 (iPSC) but different at d19
316 (NPC), d35 (imN), and d65 (GABA) (**Figure 4A**). These data suggest a diverging and
317 disrupted trajectory of GABAergic development in our DS-iPSC model when compared to
318 that in Ctl-iPSC.
319
320 To further understand the molecular regulators of dysfunctional GABAergic development in
321 DS-iPSC, we extracted the chromatin accessible peaks that were mutually exclusive in the
322 Ctl- and DS-iPSC lines at each time point (as described in the Methods section). The peaks
323 were categorized into a Ctl distinct peak list and a DS distinct peak list. In total, the Ctl
324 distinct peak list contained 3,311 accessible peaks (0 peaks at D0; 42 peaks at D19; 1,490
325 peaks at D35; and 1,779 peaks at D65), while the DS distinct peak list contained 4,434
326 accessible peaks (0 peaks at D0; 13 peaks D19; 1,708 peaks D35; and 2,713 peaks D65)
327 (**Supplementary Figure 6A**, **Figure 4B**). These distinct peaks were located at different
328 genomic regions (**Figure 4C**). Furthermore, KEGG enrichment analysis of the distinct peaks
329 at D65 revealed pathways specific to cortical neurons, such as GABAergic synapse,
330 Glutamatergic synapse, Dopaminergic synapse, and others, in Ctl-GABA but not in DS-
331 GABA (**Supplementary Figure 6B**, **Figure 4D**).
332
333 Next, we combined the distinct peak lists of the Ctl- and DS-iPSC lines and calculated
334 enrichment of TF motifs using a systematic approach with chromVAR (chromatin variation
335 across regions)[38]. We then performed a non-hierarchical clustering of TFs enriched in the
336 distinct groups and identified three clusters (Dis-1, Dis-2, Dis-3) (**Figure 4E**). Cluster Dis-1
337 comprised two subclusters of TFs: Subcluster 1 included the OCT family of TFs (OCT2,
338 OCT4, OCT6) and BRN1, with enrichment restricted to D0 (iPSC) in the DS group whereas
339 in the Ctl group the enrichment was observed at D0, D35, and D65 but not at D19. Subcluster

340 2 included the GABAergic specific TFs OLIGO2, ASCL1, NEUROD1, NEUROG2, NKX6.1,
341 LHX2, and others. These TFs were not enriched at any time-point in the DS group but
342 enriched in the control group at D35 and D65 (**Figure 4F**). In cluster Dis-2, TFs such as
343 JUNB, AP-1, RUNX2, and others were enriched in the DS group from d0 (iPSC) to D65
344 (GABA). However, in the Ctl group enrichment for Dis-2 cluster was observed only at D0
345 (iPSC). Cluster Dis-3 is enriched in both Ctl- and DS-iPSC for TFs of the TEAD family, AP-
346 2 and NF-kappa beta. In the Ctl group, this enrichment increased significantly in NPC and
347 decreased (disappeared) in imN and GABAergic neurons. Interestingly, the enrichment of
348 these TFs in cluster Dis-1 persisted in the DS group with development from NPC to GABA.
349 The absent enrichment of GABA -specific TF motifs at D65 in the DS group brings further
350 support for a disrupted chromatin remodeling during interneuron development.
351

352 **VPA induces changes in the chromatin landscape of iPSC derived GABAergic**
353 **interneurons**

354 Valproic acid (VPA) is a broad-spectrum anti-epileptic drug commonly used in the treatment
355 of DS[1]. However, the response to VPA treatment varies considerable among affected
356 individuals[39]. Prior reports suggest that the drug acts as a histone deacetylase (HDAC)
357 inhibitor and thereby impacts chromatin remodeling[22,23]. We therefore hypothesized that
358 chromatin changes induced by VPA in GABAergic cells may uncover processes contributing
359 to therapeutic effects of the drug. To this end, we cultured Ctl- and DS-iPSC-derived
360 GABAergic interneurons at D65 with and without VPA supplementation at therapeutic
361 concentrations for six days. We then performed ATAC-Seq on three sample pairs of Ctl-
362 GABA and on two pairs of DS-GABA (**Supplementary Figure 7A-D, Figure 5A)**.
363 Subsequent PCA analysis of the ATAC-Seq data showed that VPA exposure induced variable
364 changes in accessible chromatin that were seemingly iPSC-line specific (**Figure 5B, 5C,**
365 **Supplementary Figure 7E**). We then focused our analysis on the sample pairs showing the
366 most extensive VPA-induced changes in chromatin accessibility, including two Ctl-GABA
367 pairs (Ctl1B and Ctl7C) and one DS-GABA pair (DD5A; **Figure 5C**). Genomic annotation
368 revealed that chromatin changes induced by VPA were distributed in promoters, introns, and
369 distal regulatory elements and at a variable extent when comparing individual Ctl and DS
370 pairs (**Supplementary Figure 7F**). The regions showing VPA induced changes in accessible
371 chromatin were distributed in promoters, introns, and distal regulatory elements (**Figure 5D**).
372 The changes in chromatin accessibility after VPA treatment observed in both the Ctl- and DS-
373 GABA may reflect unspecific effects of the drug. To validate our hypothesis on chromatin

374 specific effects of VPA we performed enrichment analysis of differentially accessible peaks
375 for each iPSC-GABA pair. The results show enrichment in chromatin-relevant pathways in
376 both Ctl and DS pairs (**Figure 5E**). The analysis of open chromatin in response to VPA in
377 Ctl- and DS-GABA thus suggest drug-induced changes that are unspecific and genome-wide.
378 This is in line with the reported unpredictable effects of VPA on seizure frequencies in DS.
379
380 Since VPA treatment has an effect on seizure frequencies in a subgroup of affected
381 individuals, we investigated whether VPA could "restore" the chromatin accessibility profile
382 of DS-GABA into the chromatin profile of Ctl-GABA. The pathways relevant for GABAergic
383 cells became enriched in the chromatin regions that become accessible after VPA treatment in
384 the DS-GABA sample pair (**Figure 5E**). A specific analysis of TF motifs becoming
385 accessible in VPA-treated DS-GABA uncovered enriched motifs for TFs relevant for
386 GABAergic development, such as LHX3, SOX and the RFX families of TFs (**Figure 5F**).
387 Conversely, Ctl-GABA pairs showed an opposite enrichment pattern for these TF motifs upon
388 VPA treatment. Furthermore, both Ctl- and DS-GABA showed a VPA-induced increase in
389 chromatin accessibility at regulatory regions of GABAergic specific genes, such as GAD1
390 and GABRG3 (**Figure 5G**). Taken together, our iPSC model suggests that VPA has the
391 potential to dramatically interfere with and change chromatin structure in GABAergic cells.
392 These changes are likely unspecific and may affect genes important for interneuronal
393 development.
394
395
396 **Discussion**
397 The majority of cases with DS are pharmaco-resistant and there is an urgent need to improve
398 our understanding of the underlying mechanisms for the development of targeted anti-seizure
399 treatments [2,39,40]. To this end, we used our iPSC-based model of GABAergic development in
400 DS caused by heterozygous *SCN1A* variants. The model system recapitulates hallmarks of the
401 disease and we therefore reasoned that it may improve our knowledge on DS-associated
402 epigenetic changes as well as chromatin modifications induced by the commonly used anti-
403 seizure drug VPA[13,29]. Specifically, we differentiated iPSCs from healthy donors (Ctl) and
404 DS-cases towards GABAergic cortical interneurons and characterized the dynamic chromatin
405 conformational changes using ATAC-Seq. To our knowledge, this is the first study that
406 describes chromatin accessibility changes in DS-patient derived iPSC neurodifferentiation.
407 We identified common and distinct chromatin accessibility profiles when comparing iPSC of

DS patients and healthy donors at different time points of GABAergic development. As expected, the chromatin profiles of undifferentiated iPSC are similar in the two groups, with accessible peaks for TF genes maintaining a pluripotent state, such as *NANOG* and *POU5F1*. Differentiation towards a GABAergic fate shows that both Ctl and DS iPSC-lines acquire accessible chromatin peaks associated with genes enriched in pathways relevant for interneuronal development (e.g. signaling pathways, GABAergic synapse and long-term potentiation). However, our analyses uncovered increased changes in accessible peaks at the early phase (D19) of GABAergic development in DS-patient cells when compared to the control group. The genes associated with the distinct temporal changes of open chromatin in DS-patient cells are enriched in KEGG terms such as GABAergic synapse, Glutamatergic synapse and Long-term potentiation, suggesting a perturbed and seemingly accelerated initial GABAergic induction before D35. The enrichment in these pathways is lost with further differentiation of DS derived iPSC-lines and they fail to acquire the chromatin profile of Ctl GABAergic cells at D65. The aberrant chromatin profiles in our iPSC model comply with previous studies on iPSC and mice models of DS showing both transcriptional and electrophysiological changes in interneurons[9,13,41]. In our prior study, the transcriptional changes emerged predominantly after D19, the ATAC-Seq analysis in the current study show alterations in chromatin structure already at D19. This observation confirms that epigenetic changes detected by ATAC-Seq precede the transcriptional changes[30]. Furthermore, our study defines differential accessible chromatin regions and TF motifs associated with heterozygous *SCN1A* mutations, bringing further insights into disturbed interneuronal differentiation in DS. In control iPSC lines, the chromatin accessibility of motifs for TFs relevant to drive neurogenesis, such as NEUROG2, OLIG2, BRN1, increase with differentiation whereas the same regions are closing in DS derived iPSC. On the other hand, motifs of more general TFs, such as TEAD4, FOXM1, AP-2GAMMA, become either accessible or un-accessible with differentiation in control iPSC but remain closed or open in differentiating DS iPSC. This is consistent with our previous observations in DS-GABA showing dysregulated expression of *FOXM1* and of genes enriched in pathways for histone modification and cell cycle pathways[13]. Moreover, similar to the Scn1a +/- mice model, showing an intact density of cortical and hippocampal GABAergic interneurons despite impaired functions[20], our immunostainings revealed a comparable number and morphology of DS-patient and Ctl GABAergic neurons. These observations suggests that the proliferative capacity is relatively preserved during GABAergic interneuron development in DS.

Currently, valproic acid (VPA) is commonly used as one of the first line drugs in DS[1] but the response on seizure frequencies is highly variable among affected cases[42,43]. The mode of action of VPA is not fully understood but it is believed to inhibit histone deacetylases, leading to changes in chromatin states and gene expression[25,44]. In our study, we aimed to study the epigenetic effect of VPA administration on iPSC derived GABAergic neurons derived from DS patients and healthy donors. The GABAergic interneurons exposed to therapeutic concentrations of VPA for six days showed extensive changes in accessible chromatin peaks in our cultures. Projection of the chromatin changes using KEGG uncovered pathways that reflect the expected mode of action of VPA, such as *histone acetylation* and *deacetylation* and *rRNA acetylation*, of importance for transcriptional activity.

However, the VPA-induced chromatin modifications in iPSC-GABA varied considerably with biological origin and the accessibility changes linked to GABAergic development were specific or shared for individual iPSC-GABA-lines. For example, in Ctl-GABA we observe an enrichment for LHX1-3 and DLX3 motifs that changes from open to closed after VPA exposure. In contrast, DS-GABA show a somewhat opposite enrichment pattern for LHX and DLX binding motifs after VPA exposure that changes from closed to open. In mice, motifs for the LHX and DLX family of TFs are enriched in the late interneuronal development that extends postnatally[19]. In addition, Ctl-GABA show a reduction in accessible SOX-binding motifs after VPA treatment whereas DS-GABA show an opposite response, acquiring a profile more similar to the untreated Ctl-GABA. The SOX-family of TFs has a global impact on both embryonic and adult neurogenesis[45] and enrichment of SOX binding motifs are enriched in migratory interneurons[19]. These observations may suggest a mechanism by which VPA, at least in some cases, facilitates accessibility for TFs with beneficial effects on postnatal GABAergic function. Moreover, VPA treated DS-GABA uncovered enriched changes for TF motifs for AP-1 and BRN1 that made the cells acquire a pattern more similar to that in control lines. It may therefore be hypothesized that VPA induces unspecific changes in chromatin structure of iPSC-GABA that, at least in some cases, may lead to an increased accessibility for TFs linked to GABAergic development. Such a variability in response to VPA exposure in our model is consistent with the unpredictable effects of VPA on seizure-frequencies, even in individuals with identical *SCN1A* mutations[39], mediated by epigenetic factors that are specific to individuals. Our findings represent an important step forward to clarify epigenetic changes in inhibitory interneurons that are associated with the progression to DS, adding data to a frame-work of knowledge for the development of targeted and

476 personalized therapies. Further studies are now required to increase the number of
477 independent iPSC lines with *SCN1A* mutations to validate our findings on epigenetic changes
478 in DS and the effects of anti-seizure drugs such as VPA.
479
480 **Materials and Methods**
481 **Cell culture, GABAergic differentiation and sampling**
482 iPSC from three patients (DD1C, DD4A, DD5A) and three controls (Ctl1B, Ctl7C, Ctl8F)
483 were cultured on human recombinant laminin LN521 (Biolamina) in Essential-8™ medium
484 (Thermo Fisher Scientific) and passaged using Trypl Express (Thermo Fisher Scientific) as
485 described[29]. GABAergic interneuron differentiation from iPSC was performed as previously
486 described[13].
487 Cell cultures were sampled at days 0 (D0), D19, D35 and D65, respectively, by harvesting
488 cells with TryplE and collecting by centrifugation (300 x g, 3 min). Additionally, neuronal
489 cell cultures at D65 were treated with valproic acid (VPA; 0,5 mM) for 6 days and
490 subsequently harvested for analysis. Harvested cells were resuspended in 1 ml of 1 x PBS and
491 fixed by adding an equal amount of 2% formaldehyde for 10 min at room temperature. The
492 reaction was quenched by adding 100 ul 2,5 M glycine solution. Fixed cells were collected by
493 centrifugation and washed twice with 1 x PBS. Cells where then resuspended in 1 x PBS,
494 counted using an EVE automatic cell counter (EnTek) with Trypan Blue, and subsequently
495 50’000 cells/sample were processed for library preparation for ATAC sequencing.
496
497 **Tn5 transposome assembly**
498 Tn5 transposome assembly was performed by as previously described[46]. Briefly, 2 µM
499 annealed Tn5MErev/Tn5ME-A, 2 µM annealed Tn5MErev/Tn5ME-B, and 2 µM Tn5
500 transposase (Protein Science Facility at Karolinska Institutet, Stockholm) in dialysis buffer
501 (50 mM HEPES-KOH at pH 7.2, 50 mM NaCl, 0.05 mM EDTA, 0,5 mM DTT, 0.05% Triton
502 X-100, 5% glycerol) with 40% glycerol were mixed, incubated for 1 h at room temperature
503 and subsequently stored at −20°C until use. The adaptor oligonucleotides (Tn5MErev: 5'-
504 /Phos/CTGTCTCTTATACACATCT-3', Tn5ME-A: 5′ -
505 TCGTCGGCAGCGTCAGATGTGTATAAGAGACAG-3′ and Tn5ME-B: 5′-
506 GTCTCGTGGGCTCGGAGATGTGTATAAGAGACAG-3′) were synthesized by Integrated
507 DNA Technology. For oligo annealing, equimolar amounts of Tn5MErev and Tn5ME-A or
508 Tn5ME-B and Tn5MErev, respectively, were combined in a PCR tube and annealed using the
509 following program: 95°C for 5 min, ramp down to 25°C with −0.1°C/s increments.

510

511 **ATAC-Seq library preparation and sequencing**

512 ATAC-Seq libraries were prepared following[46]. In brief, two technical replicates per sample
513 containing 50,000 nuclei each were collected at 500 x g for 5 min at 4°C. Nuclei were
514 resuspended in lysis buffer (10 mM Tris-Cl, pH 7.4; 10 mM NaCl; 3 mM MgCl2; 0.1% Igepal
515 CA-630) and centrifuged at 500 x g for 10 min. The supernatant was removed and each nuclei
516 pellet was resuspended in tagmentation buffer (25 µL 2 × TD buffer) with 2.5 µl Tn5
517 transposome and incubated at 37°C for 30 min. An equal volume of 2 x reverse crosslinking
518 buffer (50 mM Tris-Cl, 1mM EDTA, 1% SDS, 0.2M NaCl, 5 ng/ml Proteinase K) was added
519 to each sample and incubated at 65°C with agitation at 1200 rpm for overnight. DNA was
520 isolated using a MinElute PCR Purification Kit (Qiagen). Sequencing libraries were prepared
521 following described standard protocol[47]. All libraries were sequenced on an Illumina Nova-
522 seq platform at Novogene Europe.

523

524 **Immunofluorescence staining**

525 Staining was performed on cells fixed with ice-cold 4% PFA and subsequently permeabilized
526 in blocking solution (1 x PBS pH 7.4, 1% BSA, 0.1% Triton X-100). Primary antibodies
527 against MAP2 (1:5'000; abcam, Cambridge, United Kingdom), GABA (1:1'000; Sigma, MO,
528 United States), GAD1 (1:100, Millipore, MA, United States) and DCX (1:100, Santa Cruz,
529 United States) were used for immunostaining and quantification. Primary antibodies were
530 allowed to bind overnight separately or in appropriate combinations at 4°C. After washing
531 three times in 1 x PBS, the secondary antibodies donkey anti-goat IgG AlexaFluor 633,
532 donkey anti-rabbit IgG AlexaFluor 568 or donkey anti-mouse IgG AlexaFluor 488 (1:1'000;
533 ThermoFisher Scientific, Waltham, MA, United States) were applied alone or in appropriate
534 combinations for 1.5 h at room temperature in the dark. Visualization was performed on a
535 Zeiss 510 confocal microscope (Carl Zeiss Microscopy, Jena, Germany) using Zen 2009
536 imaging software. Image processing was carried out using FIJI software.

537

538 **Bioinformatic and statistical analyses**

539 **ATAC-Seq data processing and quality analysis**

540 After the Adapter sequence trimming, the ATAC-Seq sequencing reads were mapped to
541 genome hg38 using bowtie2[48]. Mapped paired reads were corrected for the Tn5 cleavage
542 position by shifting +4/-5 bp depending on the read strand. All mapped reads were extended
543 to 50 bp centered around the Tn5 offset. PCR duplicates were removed using Picard

544 (http://broadinstitute.github.io/picard/), and sequencing reads from chromosome M were
545 filtered out. The Peak calling of each ATAC-Seq library was performed with MACS2[49] with
546 parameters -f BED, -g hs, -q 0.01, --nomodel, --shift 0. Peaks were merged into a matrix using
547 bedtools merge [50]. Raw reads within peaks were normalized using EdgeR's cpm function [51].
548 Log transformation was applied to these normalized peaks to calculate the Pearson correlation
549 among duplicates. Differential ATAC peaks for clusters were selected using DESeq2[52] with
550 the following cutoffs: FDR < 0.05, |log2 fold change| > 1, and peak average intensity > 16.
551

552 **Chromatin accessibility dynamic across differentiation**

553 Cluster analysis was conducted on both control and patient groups of ATAC-Seq data at
554 different time points during differentiation (D0, D19, D35, and D65). The raw data were
555 processed with background correction and normalization using Reads Per Kilobase per
556 Million mapped reads (RPKM). Clustering analysis was performed separately for the control
557 and patient groups of ATAC-Seq data using the Mfuzz package[53], with minimum standard
558 deviation and Z score parameters set at 1 and 0.5, respectively. Clusters were assigned based
559 on the chromatin accessibility patterns of differential chromatin accessible peaks.
560 Subsequently, clusters exhibiting significant changes were selected for further analysis.
561

562 **Annotation of unique ATAC peaks to genes and KEGG pathway analysis**

563 Genomic annotation of each ATAC-Seq peak to its nearest gene for the differential accessible
564 regions was done using ChIPseeker[54]. A gene promoter region was defined as 3 kb upstream
565 and 3 kb downstream of the transcription start site. The peaks were annotated to their nearest
566 gene within a 10 kb distance from the transcription start site (TSS). Subsequently,
567 Clusterprofiler[55] was used to perform Kyoto Encyclopedia of Genes and Genomes (KEGG)
568 pathway enrichment analysis, and the results were ranked by false discovery rate (FDR). An
569 FDR of less than 0.05 was set as significant.
570

571 **Transcription factors (TFs) motif enrichment analysis**

572 TF motif enrichment was performed with HOMER [56] using the differential accessible regions
573 as input. For TF binding prediction, chromVAR [38] was employed. In brief, the Homer
574 vertebrate TF database was used as input for TF motifs in chromVAR, and then TF
575 accessibility deviation values were calculated for each sample across the entire sample set. TF
576 deviations with a threshold greater than 2 were retained, and TF motifs with a positive
577 correlation with one group/cluster were selected to represent that group/cluster. TFs were

ranked based on their variability within each group/cluster, and z-scores of deviations from each TF were visualized in a heatmap.

**Author contributions**

Conceptualization: JS, ND, XC; Methodology: JS, XL, YD, JK, AW; Analysis and Investigation: JS, XL, YD, JK, ND, XC; Data curation and Visualization: JS, XL, YD, JK; Writing – original draft: JS, XC; Writing – Review and Editing: JS, XL, JK, YD, ND, XC; Supervision: ND, XC; Funding Acquisition: ND, XC.

**Declaration of interest**

The authors declare that no conflicting interest exists.

**Acknowledgements**

Research in the lab is funded by the Swedish Research Council (2020-01947 to N.D. and 2022-00658 to X.C.), Hjärnfonden (FO2020-0171 and FO2022-0042 to ND), Swedish Cancer Foundation (21 1449Pj, 22 0491 JIA to X.C.), Stiftelsen Margarethahemmet (to N.D.) and Sävstaholm Society (to J.S.), Uppsala University and Science for Life Laboratory. The funders played no role in study design, data acquisition and interpretation or decision to publish.

**Availability of the data**

The ATAC-Seq data generated for this study have been deposited in the Sequence Read Archive (SRA) with the following number: PRJNA1013337.

**References**

1 He, Z., Li, Y., Zhao, X. & Li, B. Dravet syndrome: Advances in etiology, clinical presentation, and treatment. *Epilepsy Res* **188**, 107041, doi:10.1016/j.eplepsyres.2022.107041 (2022).

2 Dravet, C. The core Dravet syndrome phenotype. *Epilepsia* **52 Suppl 2**, 3-9, doi:10.1111/j.1528-1167.2011.02994.x (2011).

3 Li, W., Schneider, A. L. & Scheffer, I. E. Defining Dravet syndrome: An essential pre-requisite for precision medicine trials. *Epilepsia* **62**, 2205-2217, doi:10.1111/epi.17015 (2021).

4 Ragona, F. Cognitive development in children with Dravet syndrome. *Epilepsia* **52 Suppl 2**, 39-43, doi:10.1111/j.1528-1167.2011.03000.x (2011).

5 Brunklaus, A. & Zuberi, S. M. Dravet syndrome--from epileptic encephalopathy to channelopathy. *Epilepsia* **55**, 979-984, doi:10.1111/epi.12652 (2014).

6 Cheah, C. S. *et al.* Specific deletion of NaV1.1 sodium channels in inhibitory interneurons causes seizures and premature death in a mouse model of Dravet syndrome. *Proc Natl Acad Sci U S A* **109**, 14646-14651, doi:10.1073/pnas.1211591109 (2012).

7 Kalume, F. *et al.* Sleep impairment and reduced interneuron excitability in a mouse model of Dravet Syndrome. *Neurobiol Dis* **77**, 141-154, doi:10.1016/j.nbd.2015.02.016

S0969-9961(15)00043-1 [pii] (2015).

8 Ito, S. *et al.* Mouse with Nav1.1 haploinsufficiency, a model for Dravet syndrome, exhibits lowered sociability and learning impairment. *Neurobiol Dis* **49**, 29-40, doi:10.1016/j.nbd.2012.08.003 (2013).

9 Han, S. *et al.* Autistic-like behaviour in Scn1a+/- mice and rescue by enhanced GABA-mediated neurotransmission. *Nature* **489**, 385-390, doi:10.1038/nature11356 (2012).

10 Yu, F. H. *et al.* Reduced sodium current in GABAergic interneurons in a mouse model of severe myoclonic epilepsy in infancy. *Nat Neurosci* **9**, 1142-1149, doi:nn1754 [pii]

10.1038/nn1754 (2006).

11 Tai, C., Abe, Y., Westenbroek, R. E., Scheuer, T. & Catterall, W. A. Impaired excitability of somatostatin- and parvalbumin-expressing cortical interneurons in a mouse model of Dravet syndrome. *Proc Natl Acad Sci U S A* **111**, E3139-3148, doi:10.1073/pnas.1411131111 (2014).

12 Sun, Y. *et al.* A deleterious Nav1.1 mutation selectively impairs telencephalic inhibitory neurons derived from Dravet Syndrome patients. *Elife* **5**, doi:10.7554/eLife.13073

e13073 [pii] (2016).

13 Schuster, J. *et al.* Transcriptomes of Dravet syndrome iPSC derived GABAergic cells reveal dysregulated pathways for chromatin remodeling and neurodevelopment. *Neurobiol Dis* **132**, 104583, doi:10.1016/j.nbd.2019.104583 (2019).

14 Maeda, H. *et al.* Establishment of isogenic iPSCs from an individual with SCN1A mutation mosaicism as a model for investigating neurocognitive impairment in Dravet syndrome. *J Hum Genet* **61**, 565-569, doi:10.1038/jhg.2016.5

jhg20165 [pii] (2016).

15 Jiao, J. *et al.* Modeling Dravet syndrome using induced pluripotent stem cells (iPSCs) and directly converted neurons. *Hum Mol Genet* **22**, 4241-4252, doi:10.1093/hmg/ddt275

ddt275 [pii] (2013).

16 Higurashi, N. *et al.* A human Dravet syndrome model from patient induced pluripotent stem cells. *Mol Brain* **6**, 19, doi:10.1186/1756-6606-6-19

1756-6606-6-19 [pii] (2013).

17 Arshad, A. *et al.* Extended Production of Cortical Interneurons into the Third Trimester of Human Gestation. *Cereb Cortex* **26**, 2242-2256, doi:10.1093/cercor/bhv074 (2016).

18 Xu, G. *et al.* Late Development of the GABAergic System in the Human Cerebral Cortex and White Matter. *J Neuropath Exp Neur* **70**, 841-858, doi:10.1097/NEN.0b013e31822f471c (2011).

19 Allaway, K. C. *et al.* Genetic and epigenetic coordination of cortical interneuron development. *Nature* **597**, 693-697, doi:10.1038/s41586-021-03933-1 (2021).

20 Ogiwara, I. *et al.* Nav1.1 haploinsufficiency in excitatory neurons ameliorates seizure-associated sudden death in a mouse model of Dravet syndrome. *Hum Mol Genet* **22**, 4784-4804, doi:10.1093/hmg/ddt331 (2013).

21 Aras, L. M., Isla, J. & Mingorance-Le Meur, A. The European patient with Dravet syndrome: results from a parent-reported survey on antiepileptic drug use in the European population with Dravet syndrome. *Epilepsy Behav* **44**, 104-109, doi:10.1016/j.yebeh.2014.12.028 (2015).

22 Ghodke-Puranik, Y. *et al.* Valproic acid pathway: pharmacokinetics and pharmacodynamics. *Pharmacogenet Genomics* **23**, 236-241, doi:10.1097/FPC.0b013e32835ea0b2 (2013).

23 Ximenes, J. C. M., Verde, E. C. L., Naffah-Mazzacoratti, M. G. & Viana, G. S. d. B. Valproic Acid, a Drug with Multiple Molecular Targets Related to Its Potential Neuroprotective Action. *Neuroscience and Medicine* **3**, 107-123, doi:10.4236/nm.2012.31016. (2012).

24 Balasubramanian, D., Pearson, J. F. & Kennedy, M. A. Gene expression effects of lithium and valproic acid in a serotonergic cell line. *Physiol Genomics* **51**, 43-50, doi:10.1152/physiolgenomics.00069.2018 (2019).

25 Jiang, X. *et al.* Sodium valproate rescues expression of TRANK1 in iPSC-derived neural cells that carry a genetic variant associated with serious mental illness. *Mol Psychiatry* **24**, 613-624, doi:10.1038/s41380-018-0207-1 (2019).

26 Wang, Y. & Li, Z. RNA-seq analysis of blood of valproic acid-responsive and non-responsive pediatric patients with epilepsy. *Exp Ther Med* **18**, 373-383, doi:10.3892/etm.2019.7538 (2019).

27 Golla, U., Joseph, D. & Tomar, R. S. Combined Transcriptomics and Chemical-Genetics Reveal Molecular Mode of Action of Valproic acid, an Anticancer Molecule using Budding Yeast Model. *Sci Rep* **6**, 35322, doi:10.1038/srep35322 (2016).

28 Balasubramanian, D., Deng, A. X., Doudney, K., Hampton, M. B. & Kennedy, M. A. Valproic acid exposure leads to upregulation and increased promoter histone acetylation of sepiapterin reductase in a serotonergic cell line. *Neuropharmacology* **99**, 79-88, doi:10.1016/j.neuropharm.2015.06.018 (2015).

29 Schuster, J. *et al.* Generation of three human induced pluripotent stem cell (iPSC) lines from three patients with Dravet syndrome carrying distinct SCN1A gene mutations. *Stem Cell Res* **39**, 101523, doi:10.1016/j.scr.2019.101523 (2019).

30 Inoue, F., Kreimer, A., Ashuach, T., Ahituv, N. & Yosef, N. Identification and Massively Parallel Characterization of Regulatory Elements Driving Neural Induction. *Cell Stem Cell* **25**, 713-727 e710, doi:10.1016/j.stem.2019.09.010 (2019).

31 Trevino, A. E. *et al.* Chromatin accessibility dynamics in a model of human forebrain development. *Science* **367**, doi:10.1126/science.aay1645 (2020).

32 de la Torre-Ubieta, L. *et al.* The Dynamic Landscape of Open Chromatin during Human Cortical Neurogenesis. *Cell* **172**, 289-304 e218, doi:10.1016/j.cell.2017.12.014 (2018).

33 Inglis, G. A. S. *et al.* Transcriptomic and epigenomic dynamics associated with development of human iPSC-derived GABAergic interneurons. *Hum Mol Genet* **29**, 2579-2595, doi:10.1093/hmg/ddaa150 (2020).

34 Maroof, A. M. *et al.* Directed differentiation and functional maturation of cortical interneurons from human embryonic stem cells. *Cell Stem Cell* **12**, 559-572, doi:10.1016/j.stem.2013.04.008

S1934-5909(13)00144-6 [pii] (2013).

35 Strano, A., Tuck, E., Stubbs, V. E. & Livesey, F. J. Variable Outcomes in Neural Differentiation of Human PSCs Arise from Intrinsic Differences in Developmental Signaling Pathways. *Cell Rep* **31**, doi:ARTN 107732

10.1016/j.celrep.2020.107732 (2020).

36 Stevanovic, M. *et al.* SOX Transcription Factors as Important Regulators of Neuronal and Glial Differentiation During Nervous System Development and Adult Neurogenesis. *Front Mol Neurosci* **14**, doi:ARTN 654031

10.3389/fnmol.2021.654031 (2021).

37 Lindtner, S. *et al.* Genomic Resolution of DLX-Orchestrated Transcriptional Circuits Driving Development of Forebrain GABAergic Neurons. *Cell Rep* **28**, 2048-+, doi:10.1016/j.celrep.2019.07.022 (2019).

38 Schep, A. N., Wu, B., Buenrostro, J. D. & Greenleaf, W. J. chromVAR: inferring transcription-factor-associated accessibility from single-cell epigenomic data. *Nat Methods* **14**, 975-978, doi:10.1038/nmeth.4401 (2017).

39 Brunklaus, A. *et al.* Time to move beyond genetics towards biomedical data-driven translational genomic research in severe paediatric epilepsies. *Eur J Paediatr Neurol* **24**, 35-39, doi:10.1016/j.ejpn.2019.12.001 (2020).

40 Brunklaus, A. *et al.* SCN1A variants from bench to bedside-improved clinical prediction from functional characterization. *Hum Mutat* **41**, 363-374, doi:10.1002/humu.23943 (2020).

41 Liu, Y. *et al.* Dravet syndrome patient-derived neurons suggest a novel epilepsy mechanism. *Ann Neurol* **74**, 128-139, doi:10.1002/ana.23897 (2013).

42 Inoue, Y. *et al.* Stiripentol open study in Japanese patients with Dravet syndrome. *Epilepsia* **50**, 2362-2368, doi:10.1111/j.1528-1167.2009.02179.x (2009).

43 Dressler, A. *et al.* Efficacy and tolerability of the ketogenic diet in Dravet syndrome - Comparison with various standard antiepileptic drug regimen. *Epilepsy Res* **109**, 81-89, doi:10.1016/j.eplepsyres.2014.10.014 (2015).

44 Baumann, C., Zhang, X., Zhu, L., Fan, Y. & De La Fuente, R. Changes in chromatin accessibility landscape and histone H3 core acetylation during valproic acid-induced differentiation of embryonic stem cells. *Epigenetics Chromatin* **14**, 58, doi:10.1186/s13072-021-00432-5 (2021).

45 Stevanovic, M. *et al.* SOX Transcription Factors as Important Regulators of Neuronal and Glial Differentiation During Nervous System Development and Adult Neurogenesis. *Front Mol Neurosci* **14**, 654031, doi:10.3389/fnmol.2021.654031 (2021).

46 Chen, X. *et al.* ATAC-see reveals the accessible genome by transposase-mediated imaging and sequencing. *Nat Methods* **13**, 1013-1020, doi:10.1038/nmeth.4031 nmeth.4031 [pii] (2016).

47 Buenrostro, J. D., Giresi, P. G., Zaba, L. C., Chang, H. Y. & Greenleaf, W. J. Transposition of native chromatin for fast and sensitive epigenomic profiling of open chromatin, DNA-binding proteins and nucleosome position. *Nat Methods* **10**, 1213-1218, doi:10.1038/nmeth.2688 nmeth.2688 [pii] (2013).

48 Langmead, B., Trapnell, C., Pop, M. & Salzberg, S. L. Ultrafast and memory-efficient alignment of short DNA sequences to the human genome. *Genome Biol* **10**, R25, doi:10.1186/gb-2009-10-3-r25 (2009).

49 Zhang, Y. *et al.* Model-based analysis of ChIP-Seq (MACS). *Genome Biol* **9**, R137, doi:10.1186/gb-2008-9-9-r137 (2008).

50 Ramirez, F., Dundar, F., Diehl, S., Gruning, B. A. & Manke, T. deepTools: a flexible platform for exploring deep-sequencing data. *Nucleic Acids Res* **42**, W187-191, doi:10.1093/nar/gku365 (2014).

51 Robinson, M. D., McCarthy, D. J. & Smyth, G. K. edgeR: a Bioconductor package for differential expression analysis of digital gene expression data. *Bioinformatics* **26**, 139-140, doi:10.1093/bioinformatics/btp616 (2010).

52 Love, M. I., Huber, W. & Anders, S. Moderated estimation of fold change and dispersion for RNA-seq data with DESeq2. *Genome Biol* **15**, 550, doi:10.1186/s13059-014-0550-8 (2014).

53 Futschik M, C. B. Noise robust clustering of gene expression time-course data. *Journal of Bioinformatics and Computational Biology*, 965-988 (2005).

54 Yu, G., Wang, L. G. & He, Q. Y. ChIPseeker: an R/Bioconductor package for ChIP peak annotation, comparison and visualization. *Bioinformatics* **31**, 2382-2383, doi:10.1093/bioinformatics/btv145 (2015).

55 Yu, G. C., Wang, L. G., Han, Y. Y. & He, Q. Y. clusterProfiler: an R Package for Comparing Biological Themes Among Gene Clusters. *Omics* **16**, 284-287, doi:10.1089/omi.2011.0118 (2012).

56 Heinz, S. *et al.* Simple combinations of lineage-determining transcription factors prime cis-regulatory elements required for macrophage and B cell identities. *Mol Cell* **38**, 576-589, doi:10.1016/j.molcel.2010.05.004 (2010).

780 **Figure legends:**

781 **Main figures:**

782 **Figure 1: Chromatin accessibility dynamic during GABAeric interneuron**
783 **differentiation**

784 **A.** Schematic illustration of GABAergic interneuron differentiation protocol. Cells from
785 iPSC differentiation were collected for ATAC-Seq. Interneuron differentiation was
786 grouped into four stages: iPSC (Day 0), neural progenitor cells; NPCs (Day 19),
787 immature neurons, imN (Day 35), GABAergic interneurons, GABA (Day 65).

788 **B.** Heatmap of four Clusters identified by time series analysis using temporal changes in
789 chromatin accessibility compared to D0 (Day 0) and other points. The signal strengths
790 were denoted by color intensities.

791 **C.** Line plot of four clusters showing the average changes in chromatin accessibility.

792 **D.** Barplot for genomic distribution of differential chromatin accessible regions for each
793 cluster.

794 **E.** Heatmap for top 10 TFs enrichment in each cluster. The significance was denoted by
795 color intensities. O-S-E-N = OCT4-SOX2-TCF-NANOG.

796 **F.** Bubble plot of KEGG pathway enrichment for each cluster. p-value and enrichment
797 were indicated.

798 **G.** Genome browser view showing representative differential chromatin accessible
799 regions at the indicated gene loci.

800

801

802

803 **Figure 2: Chromatin accessibility dynamic during GABAergic differentiation in Dravet**
804 **Syndrome patients**

805 **A.** Schematic Illustration of the design for GABAergic differentiation in Dravet
806 syndrome patients. Cells from iPSC differentiation were collected for ATAC-Seq.
807 GABAergic differentiation in Dravet Syndrome patients was grouped into four stages:
808 iPSC (Day 0), NPCs (Day 19), imN (Day 35), GABA(Day 65).

809 **B.** Heatmap of four clusters identified by time series analysis using temporal changes in
810 chromatin accessibility compared D0 (Day 0) and other points. The signal strengths
811 were denoted by color intensities

812 **C.** Line plot of four clusters showing the average changes in chromatin accessibility.

813 **D.** Barplot for genomic distribution of differential chromatin accessible regions for each
814 cluster.
815 **E.** Heatmap for top 10 TFs enrichment in each cluster. The significance was denoted by
816 color intensities. O-S-E-N = OCT4-SOX2-TCF-NANOG.
817 **F.** Bubble plot of KEGG pathway enrichment for each cluster. p-value and enrichment
818 were indicated.
819 **G.** Genome browser view showing representative differential chromatin accessible
820 regions at the indicated gene loci.
821
822
823 **Figure 3: Common chromatin accessibility features between control and Dravet**
824 **Syndrome patients during GABAergic differentiation**
825
826 **A.** Heatmap for common chromatin accessible regions detected between control and
827 Dravet Syndrome (DS) group during differentiation. Four clusters were obtained from
828 time series analysis. Representative genes are labeled on the right side of heatmap.
829 **B.** Barplot for genomic distribution of chromatin accessible regions for each cluster.
830 **C.** Bubble plot of KEGG pathway enrichment for each cluster. p-value and enrichment
831 were indicated.
832 **D.** Genome browser view showing representative chromatin accessible regions at the
833 indicated gene loci.
834 **E.** Transcription factors (TFs) deviation Z scores heatmap for unique TF enriched in each
835 cluster. Representative TFs are labeled on the right side of heatmap.
836 **F.** Representative TFs enrichment (deviation Z score) dynamics at ATAC-Seq peaks in
837 control and Dravet Syndrome (DS) group during differentiation.
838
839 **Figure 4: Unique chromatin accessibility features between control and Dravet Syndrome**
840 **patients during GABAergic differentiation**
841 **A.** Principal component analysis (PCA) plot of all ATAC-Seq from control and Dravet
842 Syndrome patients during GABAergic differentiation.
843 **B.** Heatmap showing the differential chromatin accessible peaks for comparison at each
844 time point between the control and Dravet Syndrome (DS) patients. Representative
845 genes are labeled on the right side of heatmap.

846 **C.** Barplot for genomic features of unique chromatin accessible regions at each time point
847 for the control and Dravet Syndrome (DS) patients.
848 **D.** Bubble plot of KEGG pathway enrichment at GABAeric interneuron (Day 65) for the
849 control and Dravet Syndrome (DS) patients. p-value and enrichment score were
850 indicated.
851 **E.** Heatmap showing transcription factors (TFs) enrichment at differential chromatin
852 accessible peaks for comparison at each time point between the control and Dravet
853 Syndrome (DS) patients. Representative TFs are labeled on the right side of heatmap.
854 **F.** Representative TFs enrichment (deviation Z score) dynamics at ATAC-Seq peaks in
855 control and Dravet Syndrome (DS) group during differentiation.
856
857 **Figure 5: Chromatin accessibility response in valproic acid treatment of GABAergic**
858 **interneuron**
859 **A.** Schematic illustration showing measurement of chromatin accessibility response in
860 valproic acid (VPA) treatment of GABAergic interneurons.
861 **B.** Principal component analysis (PCA) plot of ATAC-Seq with and without VPA
862 treatment of GABAergic interneuron in control and Dravet Syndrome patients.
863 **C.** Heatmap of differential chromatin accessible peaks from the VPA responsible group,
864 consisting of two control samples and one Dravet Syndrome (DS) patient sample.
865 **D.** Barplot for genomic distribution of VPA responsible accessible regions from
866 differential conditions.
867 **E.** Bubble plot of KEGG pathway enrichment for each condition. p-value and enrichment
868 were indicated.
869 **F.** TF deviation Z score heatmap for top 50 transcription factors (TFs) enriched at
870 responsible chromatin regions from differential conditions.
871 **G.** Genome browser view showing representative VPA responsible chromatin accessible
872 regions at the indicated gene loci.
873
874
875
876
877
878
879

880
881
882 **Supplementary Figure 1-7:**
883
884 **Supplementary Figure 1: Quality control of ATAC-Seq samples during GABAeric**
885 **interneuron differentiation.**
886 **A.** Representative pictures of immunofluorescent staining of Ctl-iPSC derived
887 GABAergic neurons at D65 (Ctl-GABA). The Ctl-GABA cells form networks and
888 stain positive for the neuronal markers MAP2 and double cortin (DCX), the
889 GABAergic marker γ-aminobutyric acid (GABA) and the interneuronal markers
890 somatostatin (SST), parvalbumin (PV) and glutamate decarboxylase 1 (GAD1). Size
891 bar 100 μm.
892 **B.** Pearson correlation matrix from technical duplicates of ATAC-Seq at different time
893 points.
894 **C.** Quantification of fraction of reads in peaks (FRiP) of ATAC-Seq in each condition.
895 The dotted line indicates the cutoff used.
896 **D.** Transcription start site (TSS) enrichment score of ATAC-Seq in each sample.
897 **E.** Genomic distribution of chromatin accessible peaks for each sample.
898 **F.** Principal component analysis of ATAC-Seq from each sample.
899
900
901
902 **Supplementary Figure 2: Chromatin accessibility clusters identification during**
903 **GABAeric interneuron differentiation.**
904 **A.** Volcano plots show differential accessible chromatin peaks between D0 and different
905 time points. D0 (n = 6046) vs. D19 (n = 3866); D0 (n = 8880) vs. D35 (n = 7865); D0
906 (n = 7870) vs. D65 (n = 7776). The dotted lines indicate the cutoff used to identify
907 differential ATAC-Seq peaks.
908 **B.** Variance with different numbers of clusters derived from chromatin accessibility
909 during GABAeric interneuron differentiation
910 **C.** The scaled average chromatin accessibility during GABAeric interneuron
911 differentiation from each cluster.
912 **D.** The tendency of chromatin accessibility during GABAeric interneuron differentiation
913 from each cluster.

914
915
916
917 **Supplementary Figure 3: Quality control of ATAC-Seq samples during GABAeric**
918 **interneuron differentiation in Dravet Syndrome patients.**
919 **A.** Representative pictures of immunofluorescent staining of DS-iPSC derived
920 GABAergic neurons at D65 (DS-GABA). The DS-GABA cells form networks and
921 stain positive for the neuronal markers MAP2 and double cortin (DCX), the
922 GABAergic marker γ-aminobutyric acid (GABA) and the interneuronal markers
923 somatostatin (SST), parvalbumin (PV) and glutamate decarboxylase 1 (GAD1). Size
924 bar 100 μm.
925 **B.** Pearson correlation matrix from technical duplicates of ATAC-Seq from all samples.
926 **C.** Quantification of fraction of reads in peaks (FRiP) of ATAC-Seq in each condition.
927 The dotted line indicates the cutoff was used.
928 **D.** Transcription start site (TSS) enrichment score of ATAC-Seq in each sample.
929 **E.** Genomic distribution of chromatin accessible regions for each sample.
930 **F.** Principal component analysis of ATAC-Seq from each sample.
931
932
933 **Supplementary Figure 4: Chromatin accessibility clusters identification during**
934 **GABAeric interneuron differentiation in Dravet Syndrome patients.**
935 **A.** Volcano plots show differential accessible chromatin peaks between D0 and different
936 time points. D0 (n = 7798) vs. D19 (n = 5183); D0 (n = 10154) vs. D35 (n = 7239);
937 D0 (n = 6909) vs. D65 (n = 5667). The dotted lines indicate the cutoff used to identify
938 differential ATAC-Seq peaks.
939 **B.** Variance with different numbers of clusters derived from chromatin accessibility
940 during GABAeric interneuron differentiation in Dravet Syndrome patients.
941 **C.** The scaled average chromatin accessibility during GABAeric interneuron
942 differentiation from each cluster in Dravet Syndrome patients.
943 **D.** The tendency of chromatin accessibility during GABAeric interneuron differentiation
944 from each cluster in Dravet Syndrome patients.
945
946

947 **Supplementary Figure 5: Identification of common chromatin accessibility between**
948 **control and Dravet Syndrome patients during GABAeric interneuron differentiation.**
949 **A.** Venn diagrams showing the shared and distinct accessible chromatin peaks between
950 control and patient samples.
951 **B.** Variance with different numbers of clusters derived from common accessible
952 chromatin regions between control and Dravet Syndrome patients.
953 **C.** The tendency of chromatin accessibility from common accessible chromatin regions
954 between control and Dravet Syndrome patients during GABAeric interneuron
955 differentiation.
956
957
958
959 **Supplementary Figure 6: Identification of unique accessible chromatin region between**
960 **control and Dravet Syndrome patients during GABAeric interneuron differentiation.**
961 **A.** Volcano plot of differential accessible chromatin peaks between control and Dravet
962 Syndrome (DS) patients at different stage of differentiation (NPC (Day 19), imN (Day
963 35) and GABAeric interneuron (Day 65)). Dotted lines indicate cutoff from fold
964 change and false discovery rate.
965 **B.** KEGG signal pathway enrichments from unique accessible chromatin region in
966 control and Dravet Syndrome patients at NPC (Day 19), imN (Day 35).
967
968 **Supplementary Figure 7: Valproic acid treatment reshapes chromatin accessibility of**
969 **GABAeric interneuron.**
970 **A.** Pearson correlation matrix from technical duplicates of ATAC-Seq of VPA treated
971 control and Dravet Syndrome patient group.
972 **B.** Distance matrix of ATAC-Seq from VPA treated control and Dravet Syndrome patient
973 group.
974 **C.** Quantification of fraction of reads in peaks (FRiP) of ATAC-Seq in each condition.
975 **D.** Transcription start site (TSS) enrichment score of ATAC-Seq in each sample.
976 **E.** Heatmap of differential chromatin accessible regions from VPA non-responsible
977 group, consisting of one control sample and one Dravet Syndrome (DS) patient sample.
978 **F.** Genomic distribution of chromatin accessible regions for each individual sample.
979

# Figure 1

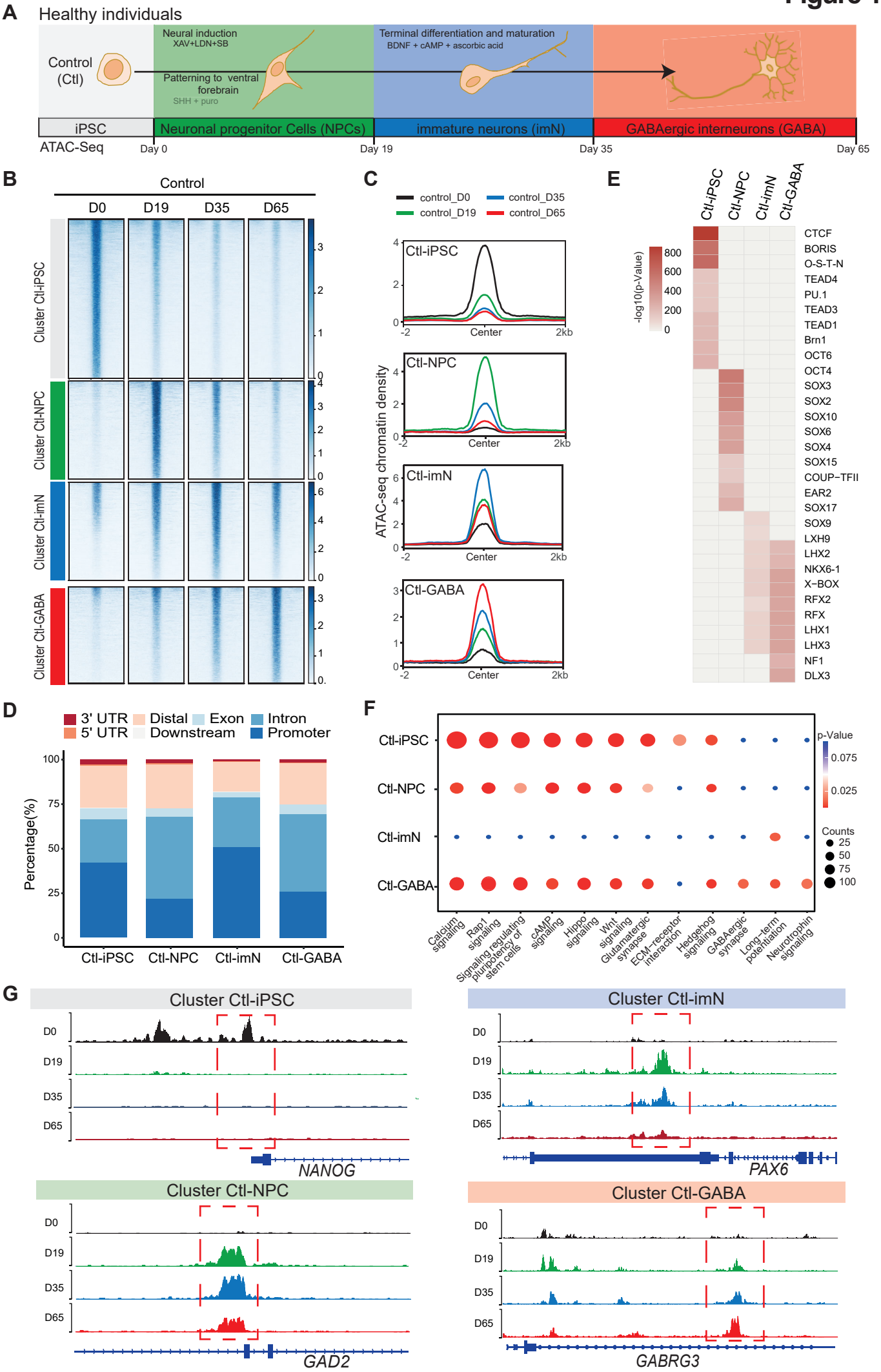
A
Healthy individuals
Control (Ctl)
Neural induction
XAV+LDN+SB
Patterning to ventral forebrain
SHH + puro
Terminal differentiation and maturation
BDNF + cAMP + ascorbic acid
iPSC
Neuronal progenitor Cells (NPCs)
immature neurons (imN)
GABAergic interneurons (GABA)
ATAC-Seq
Day 0
Day 19
Day 35
Day 65
B
Control
D0
D19
D35
D65
Cluster Ctl-iPSC
Cluster Ctl-NPC
Cluster Ctl-imN
Cluster Ctl-GABA
C
control_D0
control_D19
control_D35
control_D65
Ctl-iPSC
Ctl-NPC
Ctl-imN
Ctl-GABA
ATAC-seq chromatin density
Center
2kb
E
Ctl-iPSC
Ctl-NPC
Ctl-imN
Ctl-GABA
-log10(p-Value)
CTCF
BORIS
O-S-T-N
TEAD4
PU.1
TEAD3
TEAD1
Brn1
OCT6
OCT4
SOX3
SOX2
SOX10
SOX6
SOX4
SOX15
COUP−TFII
EAR2
SOX17
SOX9
LXH9
LHX2
NKX6-1
X−BOX
RFX2
RFX
LHX1
LHX3
NF1
DLX3
D
3' UTR
5' UTR
Distal
Downstream
Exon
Intron
Promoter
Percentage(%)
Ctl-iPSC
Ctl-NPC
Ctl-imN
Ctl-GABA
F
p-Value
Counts
Calcium signaling
Rap1 signaling
Signaling regulating pluripotency of stem cells
cAMP signaling
Hippo signaling
Wnt signaling
Glutamatergic synapse
ECM−receptor interaction
Hedgehog signaling
GABAergic synapse
Long−term potentiation
Neurotrophin signaling
G
Cluster Ctl-iPSC
NANOG
Cluster Ctl-imN
PAX6
Cluster Ctl-NPC
GAD2
Cluster Ctl-GABA
GABRG3

# Figure 2

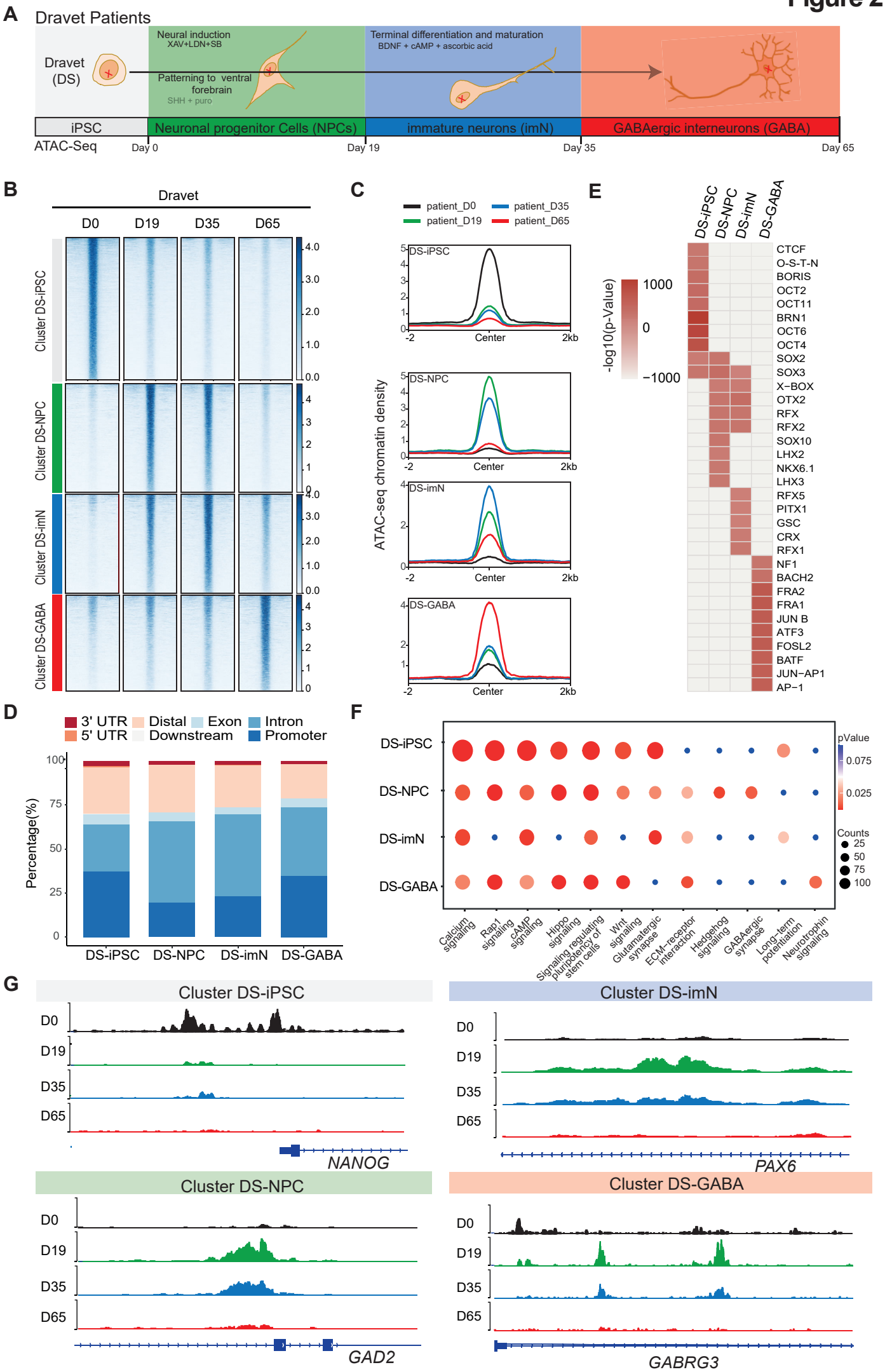
A
Dravet Patients
Dravet (DS)
Neural induction
XAV+LDN+SB
Patterning to ventral forebrain
SHH + puro
Terminal differentiation and maturation
BDNF + cAMP + ascorbic acid
iPSC
Neuronal progenitor Cells (NPCs)
immature neurons (imN)
GABAergic interneurons (GABA)
ATAC-Seq
Day 0
Day 19
Day 35
Day 65
B
Dravet
D0
D19
D35
D65
Cluster DS-iPSC
Cluster DS-NPC
Cluster DS-imN
Cluster DS-GABA
C
patient_D0
patient_D19
patient_D35
patient_D65
DS-iPSC
DS-NPC
DS-imN
DS-GABA
ATAC-seq chromatin density
Center
2kb
E
DS-iPSC
DS-NPC
DS-imN
DS-GABA
-log10(p-Value)
1000
0
−1000
CTCF
O-S-T-N
BORIS
OCT2
OCT11
BRN1
OCT6
OCT4
SOX2
SOX3
X−BOX
OTX2
RFX
RFX2
SOX10
LHX2
NKX6.1
LHX3
RFX5
PITX1
GSC
CRX
RFX1
NF1
BACH2
FRA2
FRA1
JUN B
ATF3
FOSL2
BATF
JUN−AP1
AP−1
D
3' UTR
5' UTR
Distal
Downstream
Exon
Intron
Promoter
Percentage(%)
DS-iPSC
DS-NPC
DS-imN
DS-GABA
F
pValue
0.075
0.025
Counts
25
50
75
100
Calcium signaling
Rap1 signaling
cAMP signaling
Hippo signaling
Signaling regulating pluripotency of stem cells
Wnt signaling
Glutamatergic synapse
ECM−receptor interaction
Hedgehog signaling
GABAergic synapse
Long−term potentiation
Neurotrophin signaling
G
Cluster DS-iPSC
Cluster DS-imN
Cluster DS-NPC
Cluster DS-GABA
NANOG
PAX6
GAD2
GABRG3

# Figure 3

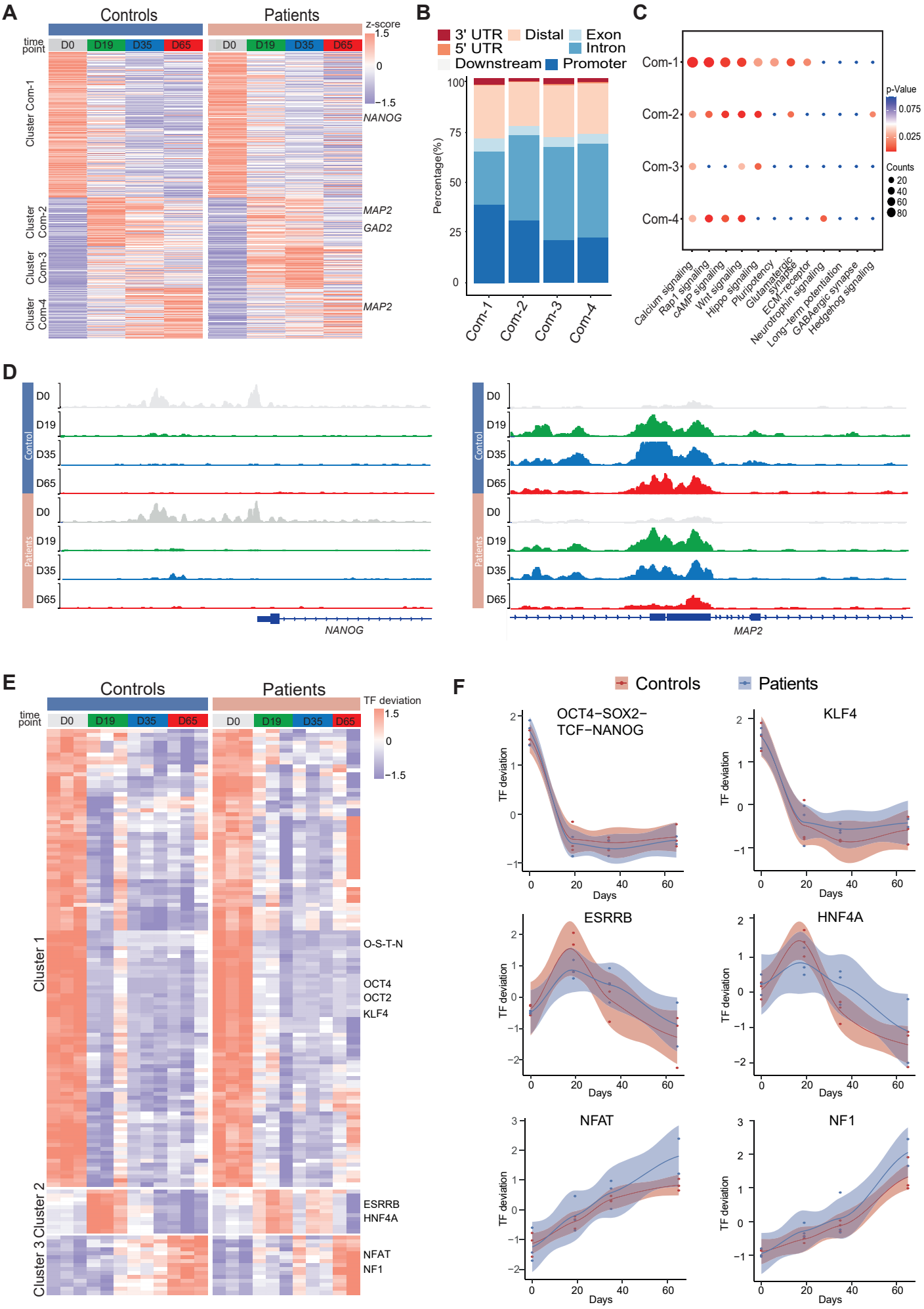
A
Controls
Patients
time point
D0
D19
D35
D65
z-score
1.5
0
−1.5
Cluster Com-1
Cluster Com-2
Cluster Com-3
Cluster Com-4
NANOG
MAP2
GAD2
MAP2
B
3' UTR
5' UTR
Distal
Downstream
Exon
Intron
Promoter
Percentage(%)
100
75
50
25
0
Com-1
Com-2
Com-3
Com-4
C
Com-1
Com-2
Com-3
Com-4
p-Value
0.075
0.025
Counts
20
40
60
80
Calcium signaling
Rap1 signaling
cAMP signaling
Wnt signaling
Hippo signaling
Pluripotency
Glutamatergic synapse
ECM−receptor
Neurotrophin signaling
Long−term potentiation
GABAergic synapse
Hedgehog signaling
D
Control
Patients
D0
D19
D35
D65
NANOG
MAP2
E
Controls
Patients
time point
TF deviation
1.5
0
−1.5
Cluster 1
Cluster 2
Cluster 3
O-S-T-N
OCT4
OCT2
KLF4
ESRRB
HNF4A
NFAT
NF1
F
Controls
Patients
OCT4−SOX2−TCF−NANOG
KLF4
ESRRB
HNF4A
NFAT
NF1
TF deviation
Days

# Figure 4

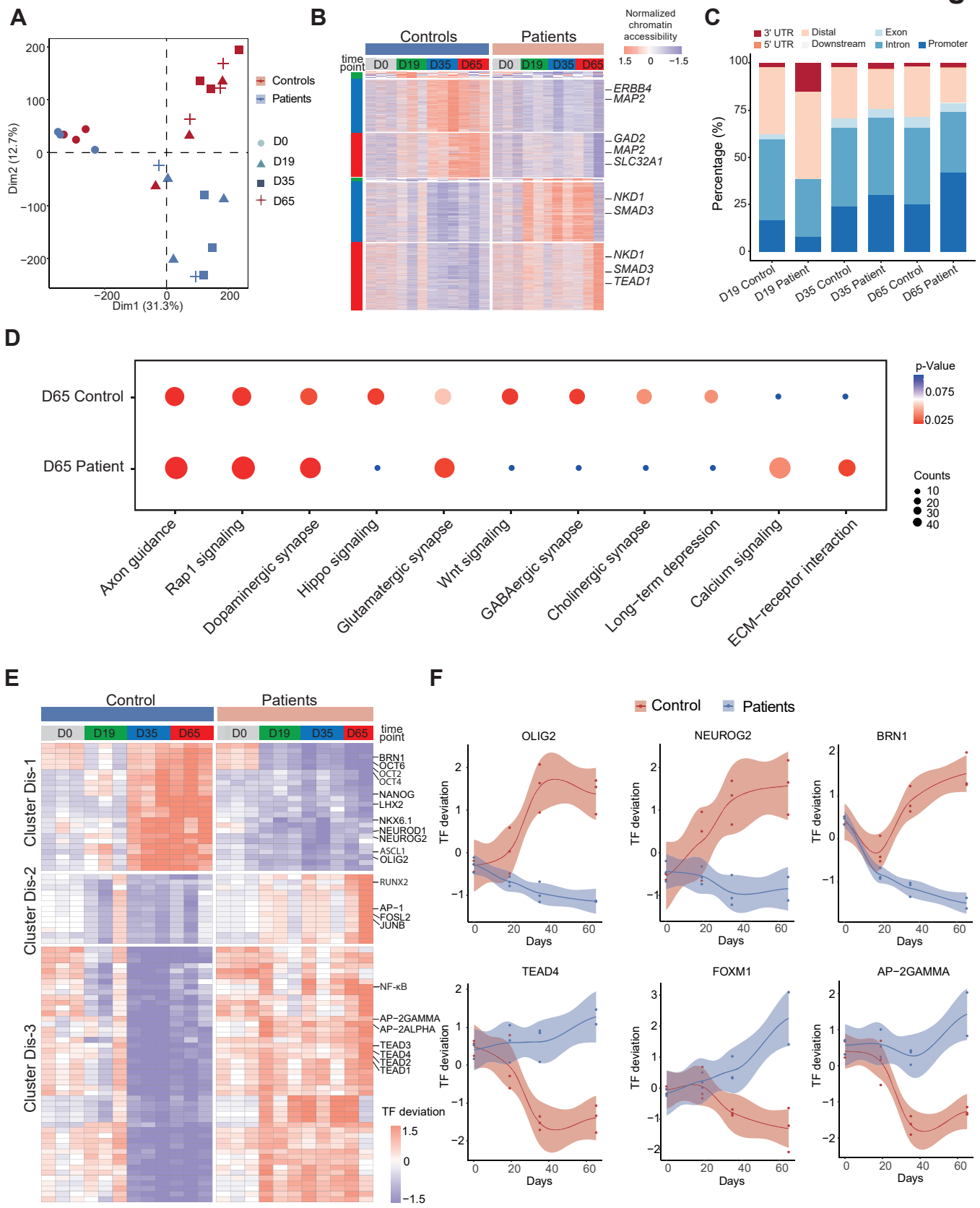
A
Dim2 (12.7%)
Dim1 (31.3%)
Controls
Patients
D0
D19
D35
D65
B
Controls
Patients
time point
D0 D19 D35 D65 D0 D19 D35 D65
Normalized chromatin accessibility
1.5 0 −1.5
ERBB4
MAP2
GAD2
MAP2
SLC32A1
NKD1
SMAD3
NKD1
SMAD3
TEAD1
C
3' UTR
5' UTR
Distal
Downstream
Exon
Intron
Promoter
Percentage (%)
D19 Control
D19 Patient
D35 Control
D35 Patient
D65 Control
D65 Patient
D
D65 Control
D65 Patient
p-Value
0.075
0.025
Counts
10
20
30
40
Axon guidance
Rap1 signaling
Dopaminergic synapse
Hippo signaling
Glutamatergic synapse
Wnt signaling
GABAergic synapse
Cholinergic synapse
Long−term depression
Calcium signaling
ECM−receptor interaction
E
Control
Patients
D0 D19 D35 D65 D0 D19 D35 D65
time point
Cluster Dis-1
Cluster Dis-2
Cluster Dis-3
BRN1
OCT6
OCT2
OCT4
NANOG
LHX2
NKX6.1
NEUROD1
NEUROG2
ASCL1
OLIG2
RUNX2
AP−1
FOSL2
JUNB
NF-κB
AP−2GAMMA
AP−2ALPHA
TEAD3
TEAD4
TEAD2
TEAD1
TF deviation
1.5
0
−1.5
F
Control
Patients
OLIG2
NEUROG2
BRN1
TEAD4
FOXM1
AP−2GAMMA
TF deviation
Days

# Figure 5

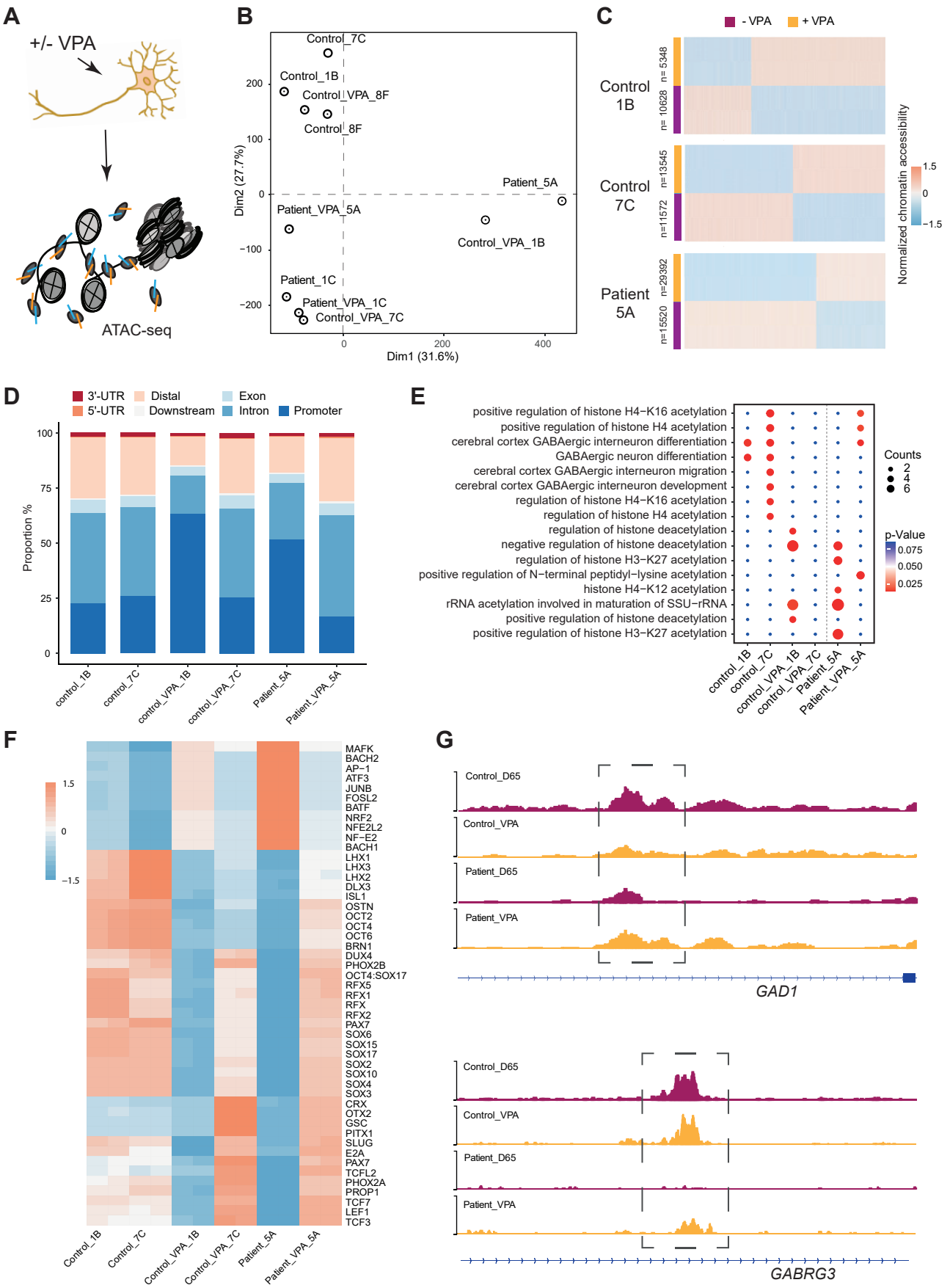
A
+/- VPA
ATAC-seq
B
Control_7C
Control_1B
Control_VPA_8F
Control_8F
Patient_5A
Patient_VPA_5A
Control_VPA_1B
Patient_1C
Patient_VPA_1C
Control_VPA_7C
Dim2 (27.7%)
Dim1 (31.6%)
C
- VPA
+ VPA
Control 1B
Control 7C
Patient 5A
n= 5348
n= 10628
n=13545
n=11572
n=29392
n=15520
Normalized chromatin accessibility
D
3'-UTR
5'-UTR
Distal
Downstream
Exon
Intron
Promoter
Proportion %
control_1B
control_7C
control_VPA_1B
control_VPA_7C
Patient_5A
Patient_VPA_5A
E
positive regulation of histone H4−K16 acetylation
positive regulation of histone H4 acetylation
cerebral cortex GABAergic interneuron differentiation
GABAergic neuron differentiation
cerebral cortex GABAergic interneuron migration
cerebral cortex GABAergic interneuron development
regulation of histone H4−K16 acetylation
regulation of histone H4 acetylation
regulation of histone deacetylation
negative regulation of histone deacetylation
regulation of histone H3−K27 acetylation
positive regulation of N−terminal peptidyl−lysine acetylation
histone H4−K12 acetylation
rRNA acetylation involved in maturation of SSU−rRNA
positive regulation of histone deacetylation
positive regulation of histone H3−K27 acetylation
Counts
p-Value
F
MAFK
BACH2
AP−1
ATF3
JUNB
FOSL2
BATF
NRF2
NFE2L2
NF−E2
BACH1
LHX1
LHX3
LHX2
DLX3
ISL1
OSTN
OCT2
OCT4
OCT6
BRN1
DUX4
PHOX2B
OCT4:SOX17
RFX5
RFX1
RFX
RFX2
PAX7
SOX6
SOX15
SOX17
SOX2
SOX10
SOX4
SOX3
CRX
OTX2
GSC
PITX1
SLUG
E2A
PAX7
TCFL2
PHOX2A
PROP1
TCF7
LEF1
TCF3
G
Control_D65
Control_VPA
Patient_D65
Patient_VPA
GAD1
GABRG3

Supp Figure 1

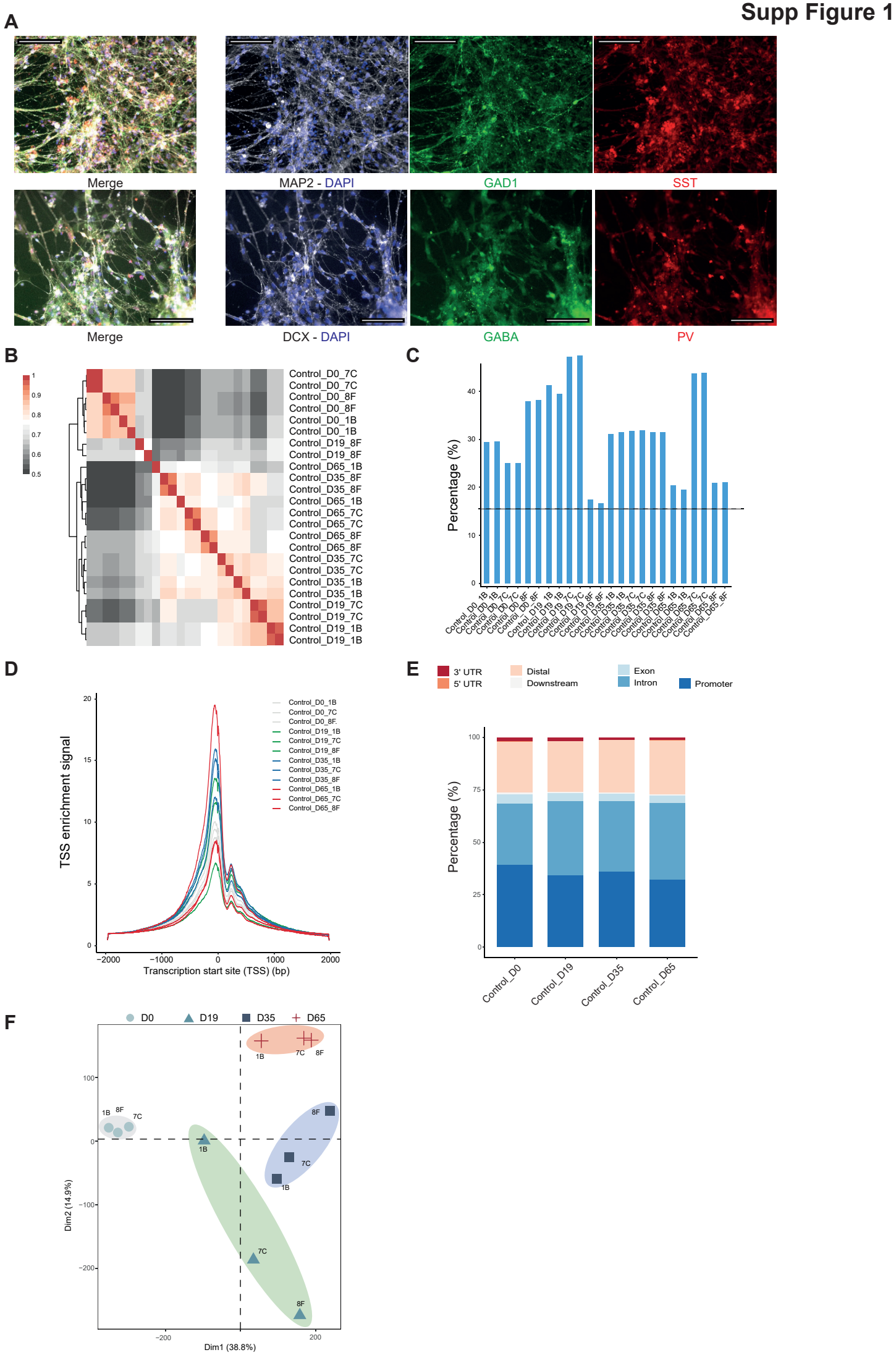

# Supp Figure 2

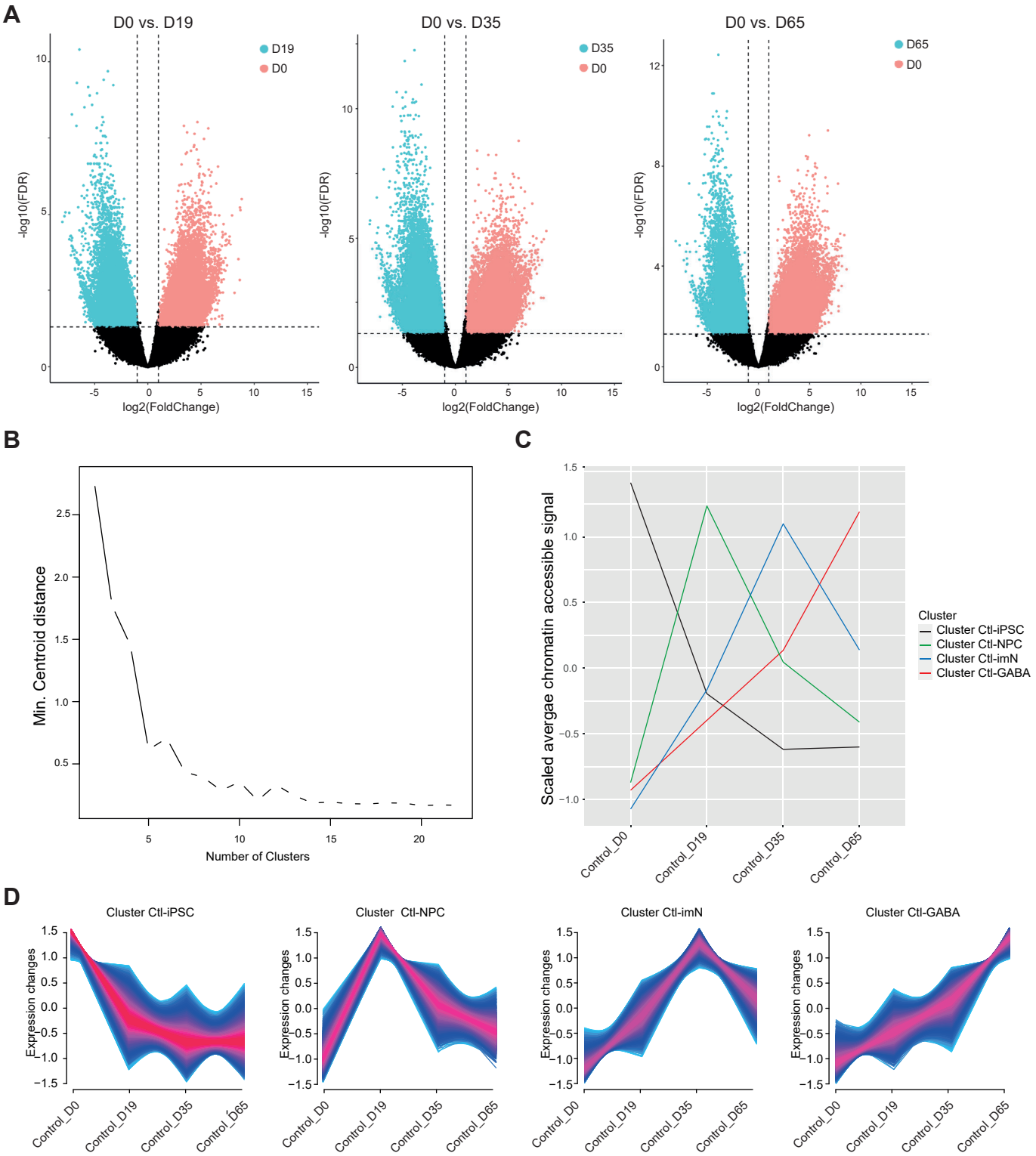

# Supp Figure 3

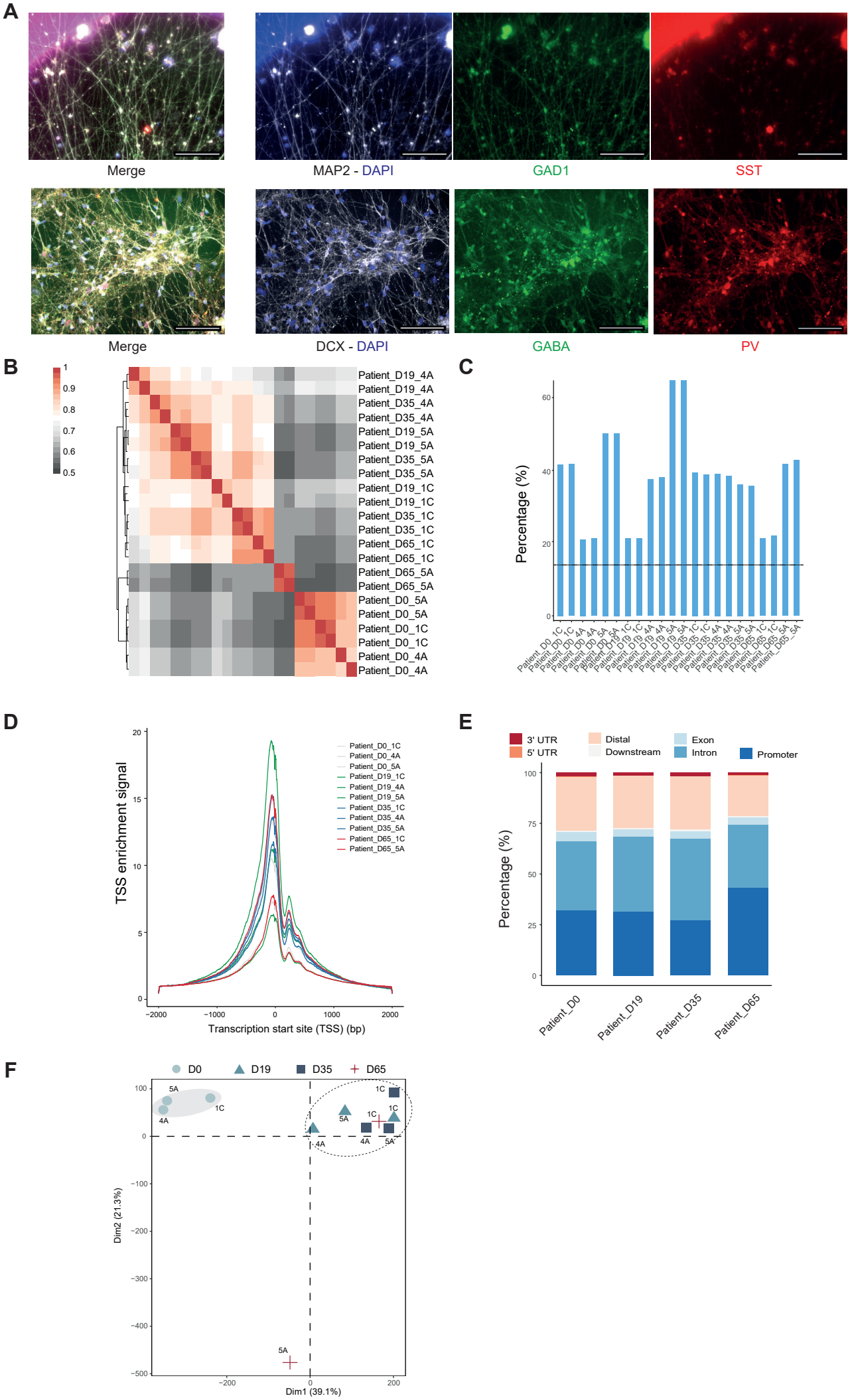

# Supp Figure 4

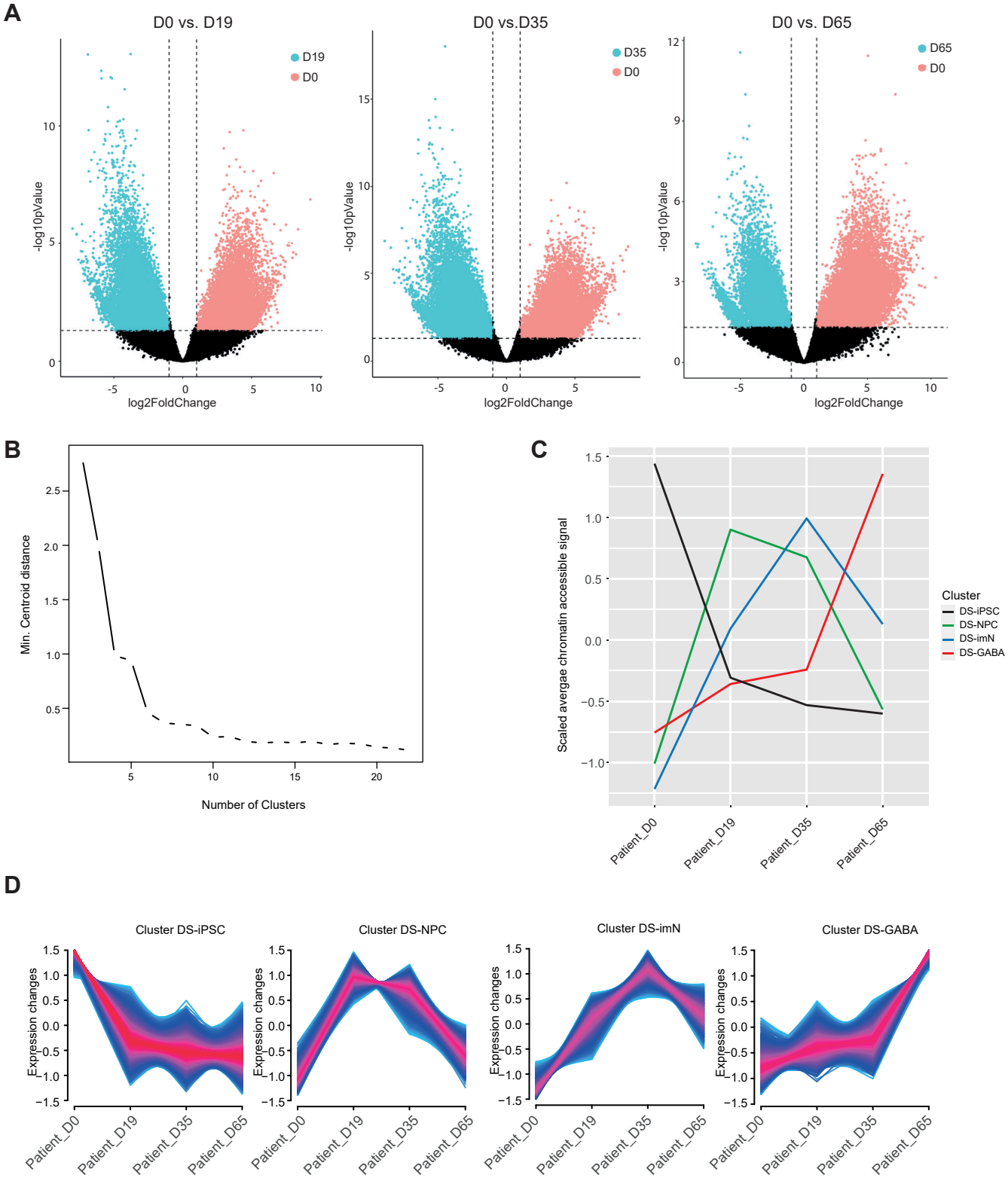

# Supp Figure 5

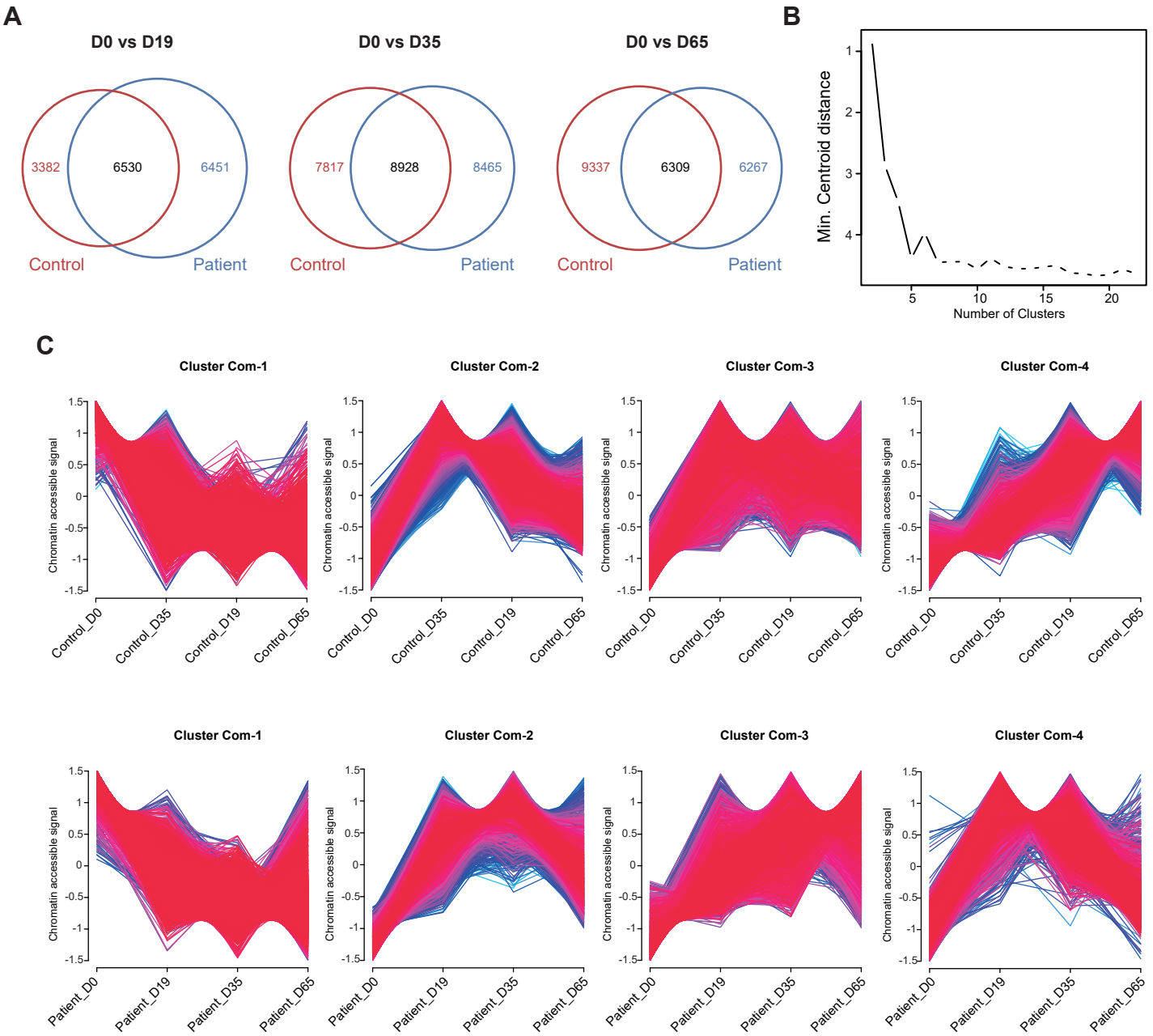

# Supp Figure 6

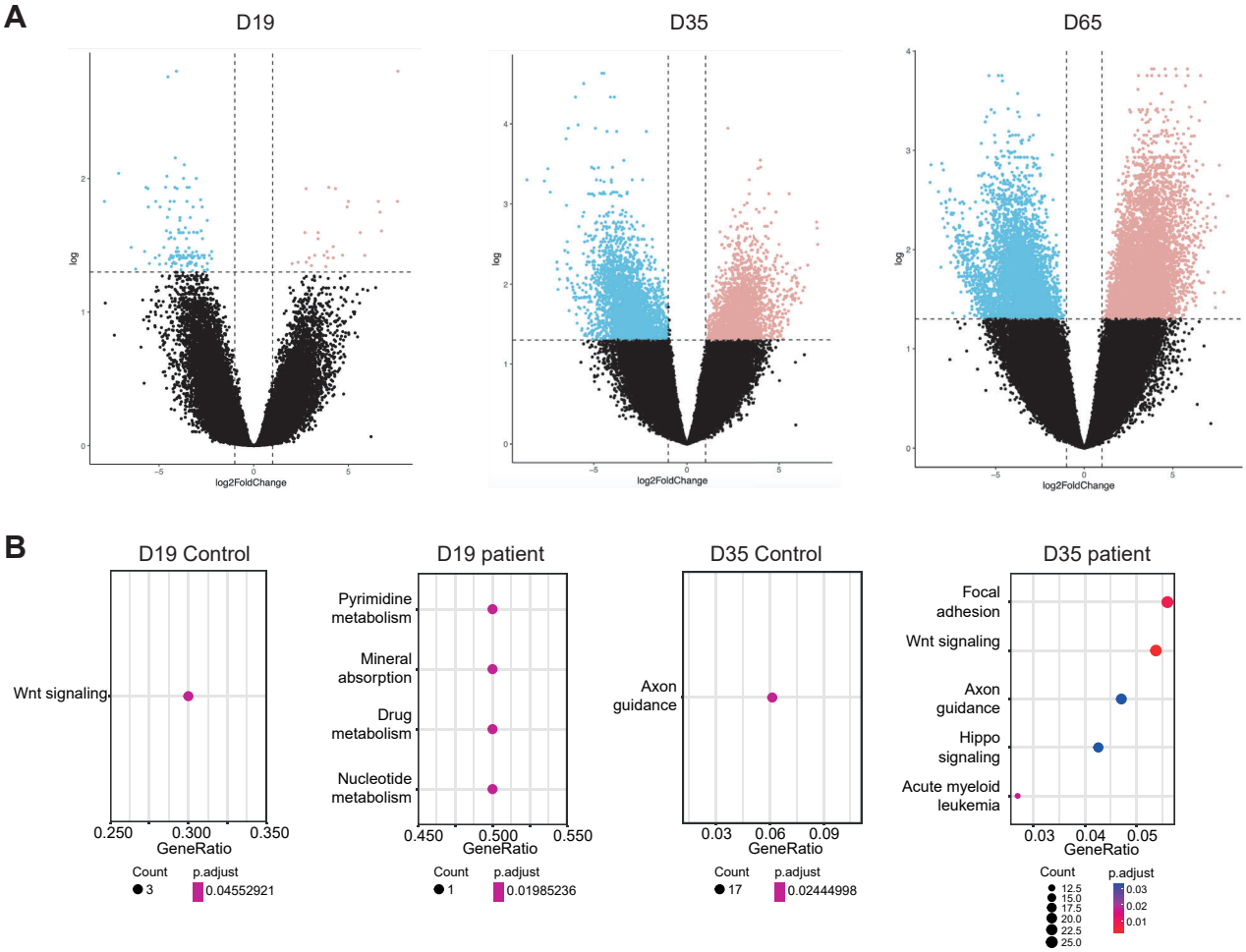
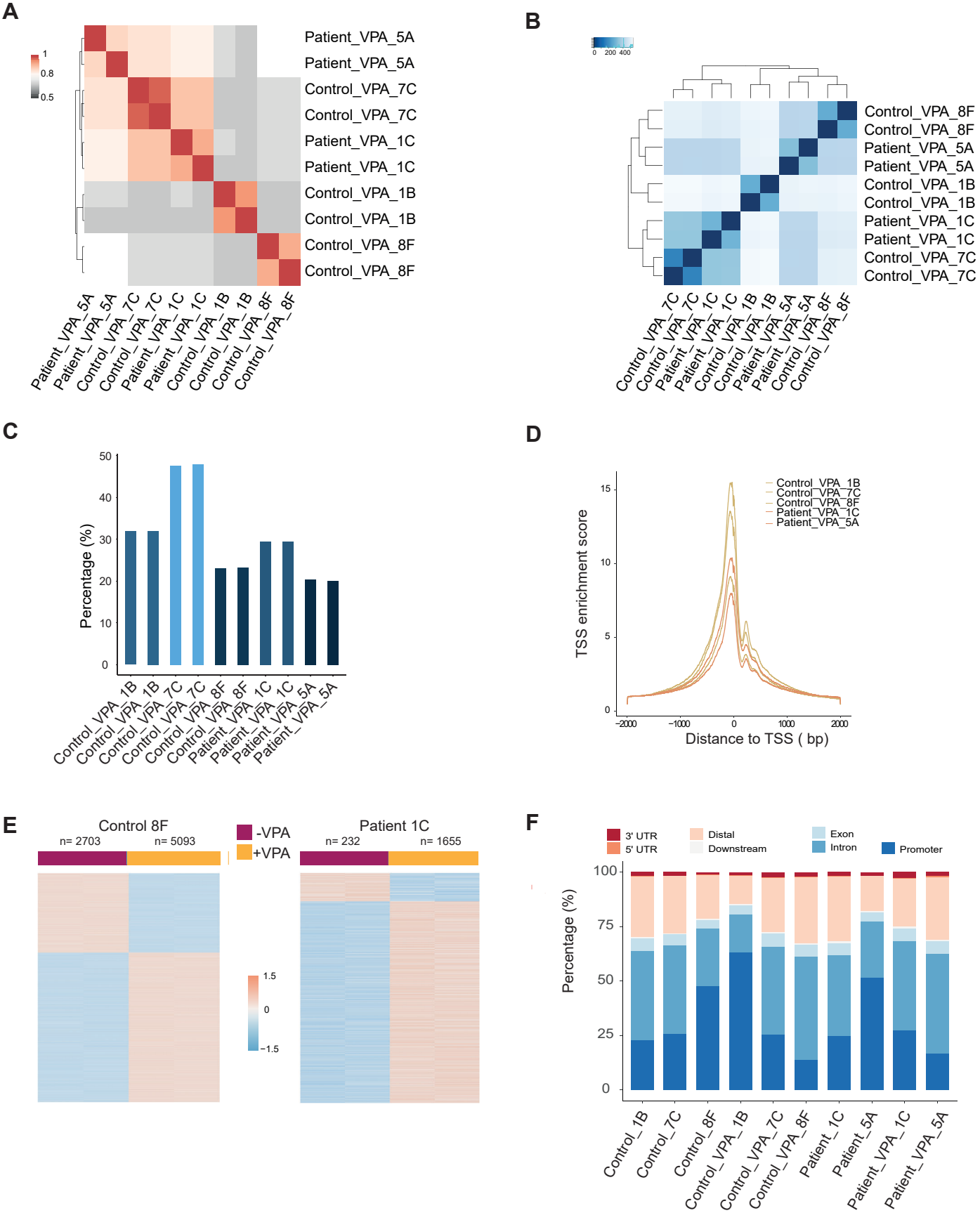
# Supp Figure 7